# Quarks and hadrons in the real space

## Volodymyr Krasnoholovets

Institute of Physics, National Academy of Sciences of Ukraine,
Stohna Nauky 46, UA-03028 Kyiv, Ukraine
*E-mail:* krasnoh@iop.kiev.ua

### Abstract

The paper reviews major approaches to the description of subatomic particles, such as leptons, quarks, hadrons and nucleons. Among these approaches are quantum chromodynamics, soliton models, bag models and others. The main accent is on a theory of the real physical space that acts as a scene on which all high-energy events take place. We discuss how a lepton and quark appear in the space constituted as a tessellation lattice of primary topological balls – the only structure that mathematics (i.e. set theory, topology and fractal geometry) offers to the constitution of ordinary physical space. Since leptons and quarks emerge in the tessellattice from a topological ball, they must interact with this substrate. The principles of the interaction of subatomic particles with space and through space between themselves are considered in detail. The approach: i) states that real quarks possess the integer charge $\pm e$ and they periodically change to the monopole state (hence, canonical particles are dynamic dyons); ii) naturally solves the problem of confinement of quarks; iii) reveals the dynamics of quarks in hadrons; iv) discloses an inner structure of the proton and neutron; v) calculates the radius of the proton; and vi) derives the nuclear forces as the result of both direct coalescence of surfaces of the nucleons and the overlapping of spatial excitations (named *inertons*) generated by the nucleons at their motion through the tessellattice. Experimental results showing nuclear transformations in samples affected by artificially generated inerton fields are demonstrated.

**Key words:** quark, lepton, quantum chromodynamics, space, tessellattice, nucleon, proton, nuclear forces, inerton

**PACS:** 12.10.-g, 12.38.Aw, 12.40.-y, 12.60.-I, 13.75.Cs, 21.30.-x, 25.00.00

# 1. Introduction

In fundamental physics the Standard Model is treated as a basic model for the description of elementary particles (see, e.g. Refs. 1). Three kinds of elementary particles are leptons, namely: electron, muon and $\tau$-lepton; besides, each lepton has its own neutrino. Quarks with three colors (red, yellow, blue) and six flavors are u, d, c, s, t, b. Each lepton and quark has the appropriate antiparticle. Leptons and quarks are fundamental fermions. The electric charges of leptons are $\pm e$, though by definition quarks are characterized by the friction electric charges $\pm e/3$ and $\pm e2/3$. The spin of leptons and quarks is the same, 1/2. Quarks and leptons are treated as point particles [2].

Leptons are able to interact through quanta of electroweak interactions, which are the photon $\gamma$ and $W^\pm$ and $Z^0$ bosons. Quarks interact through quanta of strong interactions, which are gluons, and can also interact through $W^\pm$ and $Z^0$ bosons. All these quanta are called fundamental bosons.

The Standard Model includes a primary particle called the Higgs boson, which is needed for an abstract formalism to launch a family of massive particles.

A theory of hadrons was developing from earliest partons to modern confinement. The parton model was proposed by Feynmann [3] to analyze high-energy hadron collisions. Later on it was found that partons describe the same objects now known as quarks and gluons. Literature on quarks and the appropriate science known as quantum chromodynamics (QCD) is very rich (see, e.g. monographs [4,5]). QCD studies different aspects of the interaction of quarks and hadrons.

On the other hand, one can read an interesting remark in Ref. 6: Jets probing the deep structure of hadrons reveal that at scales down to $10^{-18}$ m matter indeed shows a quark-gluon structure; however, QCD used at the analysis of the results is working with a precision of only at a level of around 10%.

There also exist other approaches describing the behavior of quarks in hadrons, which try to bring some physical ideas into the highly abstract formalism of QCD. In the present work we briefly review approaches based on QCD, the Nambu–Jona-Lasinio model [7, 8], the Skyrme model [9, 10], the MIT bag model [11-14] and the topological soliton model [15], which are most accepted among physicists.

Nevertheless, in the foreground of particle physics, a significant gap remains in understanding the causes of the stability of baryons, the quark confinement, the nature of spin-1/2 of baryons and the origin of nuclear forces. The formalism of QCD was developed based on quantum mechanics and quantum electrodynamics, which themselves were elaborated in abstract phase spaces, not the ordinary physical space. The standard model of particle physics combines all fundamental interactions in a unified theory (*the theory of everything*). However, doing so the theory of everything rests on complete undetermined basic notions, such as mass, particle, charge, lepton, quark, Compton wavelength, de Broglie wavelength, wave-particle, matter waves, wave $\psi$-function, spin, Pauli principle, etc. So, we have to keep in mind the necessity of the *theorem of something*, which will clarify the fundamental notions of quantum physics. Such a clarification can be possible only within the constitution of the real physical space in which all physical processes occur. However, the study of physical space and its relationship with the fundamental notions of quantum physics have so far been beyond the study of particle physics.

Based on previous works of the author, it will be shown below how a theory of the real physical space [16-19] and the submicroscopic concept [20-27] (which was proven experimentally, see e.g. Ref. 28) allow us to unveil the mentioned issues in detail.

## 2. QCD

In 1970s Wilczek discovered a new dynamic principle called antiscreening, or asymptotic freedom. Wilczek [29] describes this principle as follows. Color charge of a quark builds up its power to drive the strong interaction by accumulating a growing cloud at larger distances. As the virtual particles in space respond to the altered situation they rebuild a new cloud, moving along with the quark. The theories that may display such behavior, i.e. asymptotic freedom, are called nonabelian gauge theories, or Yang-Mills theories. These theories generalize quantum electrodynamics in such a way that they postulate the existence of several different kinds of charge, with complete symmetry among them. So instead of one entity, "charge", the theories use several "colors". Besides, the theory suggests a family of color gluons (instead of one photon, as is the case in electrodynamics). The color gluons themselves carry color charges. Hence the nonabelian theories differ from electrodynamics in which the photon is electrically neutral. Gluons in nonabelian theories play a more complicated role in the dynamics of these theories than do photons in electrodynamics and it is the effect of virtual gluons that is responsible for antiscreening/asymptotic freedom (which is unknown in quantum electrodynamics). Asymptotical freedom allowed the construction of a theory of the strong interaction, which describes baryons, based on three quarks, and mesons, based on quark and antiquark. This becomes possible in QCD, as the color charges of three different quarks gathered together can cancel. Three colors exhaust all possibilities, which brings us to the gauge group $SU(3)$, with three colors, and eight gluons.
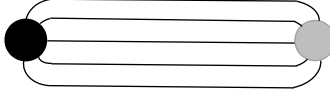
Figure 1: Confinement phenomenon: two quarks are stretched forming a "string" in which their gluon interaction becomes proportional to the distance $R$ between them. The longer the string, the stronger the attraction between the quarks.

In QCD the problem of coupling of quarks is considered in the framework of the gauge field theory that describes the strong interactions of colored quarks and gluon fields and the appropriate Lagrangian is given by

$$L = \sum_n \bar{\psi}_{n,\,a} \left( i\gamma^\mu \partial_\mu \, - \, g\gamma^\mu t_a A_\mu^C \right) \psi_{n,\,a} - \sum_n \bar{\psi}_{n,\,a} m_n \, \psi_{n,\,a} - \tfrac{1}{4} G_{\mu\nu}^A G^{A\,\mu\nu} \tag{1}$$

where repeated indices ($n$, $\mu$, and $\nu$) are summed over. Here, $\gamma^\mu$ are the Dirac $\gamma$-matrices. The $\psi_{n,\,a}$ are Dirac spinors of the quark field of flavor $n$ and mass $m_n$, with a color-index $a = 1, 2, 3$ (quarks come in three colors); $A_\mu^C$ is the four potential of the gluon fields, $C = 1, \ldots, 8$ there are 8 kinds of gluons; the color field tensor is

$$G_{\mu\nu}^a = \partial_\mu A_\nu^C - \partial_\nu A_\mu^C - g f_{ABC} \, A_\mu^B A_\nu^C; \tag{2}$$

$f_{ABC}$ are structure constants of the SU(3) color group; $t_a$ are matrices, which are generators of the SU(3) group; $g = \sqrt{4\pi\alpha_s}$ ($\hbar = c = 1$) is the color charge, i.e. an effective constant of the strong force interaction.

A first-order perturbative QCD calculation, which is valid at very large transferred four-momentum $Q$, gives for the effective constant [30,31]

$$\alpha_s(Q^2) = \frac{1}{b \ln(Q^2/\Lambda_{\mathrm{QCD}}^2)} + ..., \tag{3}$$

where the free parameter in QCD, or the QCD scale parameter $\Lambda_{\mathrm{QCD}}$, which refers to a particular definition of the effective coupling, may vary from 0.1 to 0.5 GeV, though researchers tend to the value of $\Lambda_{\mathrm{QCD}} = 217 \pm 25$ MeV [32] or rather 220 MeV [33]. Bethke [33] emphasizes that if $Q^2$ becomes larger, $\alpha_s(Q^2)$ asymptotically decreases to zero, but the constant $\alpha_s(Q^2)$ increases at smaller $Q^2$; for example, in the case of the $Z^0$ boson whose energy is 90 GeV, the constant $\alpha_s(Q^2)|_{90\ \mathrm{GeV}} = 0.12$ and $\alpha_s(Q^2)|_{35\ \mathrm{GeV}} = 0.14$ [34]. Bethke [33] mentions that $\alpha_s(Q^2)$ can exceed unity for energies in the range 100 MeV to 1 GeV; the energy scale below the order of 1 GeV is called the non-perturbative region where confinement sets in.

The spatial separation between quarks goes as

$$\lambda = \hbar/Q. \tag{4}$$

Expressions (3) and (4) show that at a very short distance and high value of $Q$ coupling between quarks decreases, vanishing asymptotically. At the limit of very large $Q$, quarks can be considered to be "free", which is called an asymptotic freedom. On the other hand, at large distances, the inter-quark coupling increases and in this case it becomes impossible to detach individual quarks from a hadron, which is called a confinement.

The confinement is interpreted by the shrinking of gluon fields in an elastic string (Fig. 1). The potential energy of a static $q\bar{q}$ pair grows with the quark-antiquark distance $r$ as
$$V(r) = \sigma r. \tag{5}$$

The string tension $\sigma$ is computed in continuum QCD. The inputs are the standard values of the vacuum condensates. The output is $\sqrt{\sigma} \approx 0.5$ GeV and is very insensitive to quarks. Numerical simulations on a lattice confirmed expression (5).

The lattice approach to QCD means that each quark occupies its own site (or does not occupy it) in an abstract spatial lattice (see, e.g. Ref. 35, 36): the quark field is defined on individual points $x$ of the lattice and the appropriate quark is connected with the neighbors by links $[x, \; x \pm a\,e_\mu]$ where $\mu$ is the Lorentz index and $a$ is the size of the meshes of the lattice. A typical lattice constant $a = 0.05 - 0.1$ fm is essential for accurate QCD simulations, though $a \approx 0.3 - 0.4$ fm also works quite well; the challenge is to make the lattice spacing as large as possible while keeping the discretization errors in the order of a few percent.

Non-perturbative gauge theory intractable calculations being considered on the lattice QCD allow one to evaluate the path integral by stochastic simulation techniques.

String excitation energies can be estimated by the Wilson loop correlation function (see, e.g. Refs. 37-39). Wilson loops are essentially phase factors in gauge theories. Wilson loops in QCD are associated with the phenomenon of a phase change known as the Aharonov–Bohm effect [40] in quantum physics. QCD can be reformulated by using the Wilson loops in a manifest gauge-invariant way.

Basically the static quark potential (5) can be presented by an asymptotic expansion [41]

$$V(r) = \sigma\,r \; - \; \alpha/r \; + \; \mu_{\mathrm{r-d}} \; + O\,(1/r^2), \tag{6}$$

where $\alpha/r$ is the quantum correction that characterizes the relativistic bosonic string (Fig. 1) and $\mu_{\mathrm{r-d}}$ is a regularization-dependent mass.

The string tension $\sigma$ is the subject of intensive theoretical and experimental studies (see, e.g. Refs. 42, 43 and also works [44, 45]). The value of $\sigma$ is evaluated as a function of temperature and the string tension points compared with the behavior of parameters of ferromagnets and superconductors relating them to confinement.

The confinement of quarks is a big challenge and researchers for more than 30 years try to describe it suggesting most fundamental approaches [44, 45]. Greensite [44] reviewed the confinement problem in $SU(\mathrm{N})$ lattice gauge theory. He notes that a popular definition of the confinement is based on the fact that all the low-lying hadrons fit nicely into a scheme in which the constituent quarks combine in a color-singlet. No particles or gluons exist in a color non-singlet state. This actuality allows one to identify the confinement with the more general concept of color confinement, which means that all asymptotic particles are color singlets. The linear potential $V(r) \sim \sigma\,r$ is only one of a number of properties of the confining force; a complete list includes the following: linearity of the static potential, Casimir scaling, N-ality dependence, and string behavior: roughening. Vortex-limited Wilson loops can be responsible for confinement to percolate through the lattice, though this creates a difficulty associated with finite temperature (because in the time direction the length of the lattice constant plays the role of inverse temperature and the change of the length will represent a transition from the confining to the deconfining phase).

One of the oldest proposals for quark confinement is the confinement as an effect due to abelian monopoles [44]; the idea is motivated by the squeezing of magnetic fields into flux tubes in type II superconductors, and by the demonstrable confinement of heavy electric charge in a monopole plasma, which arises in compact quantum electrodynamics in D = 3 dimensions. Greensite [44] emphasizes the necessity of centre symmetry: the existence of a finite string tension is related to the behavior of the centre vortex free energy; the asymptotic string tension of static quarks depends on their color charge only through the transformation properties of the quarks under the centre subgroup.

't Hooft [46] reviews new ideas on dynamic mechanisms of the absolute confinement, such as i) stipulated by the lattice structure of QCD, ii) specified by a topological phenomenon, iii) caused by a chain of gluons and iv) given by a renormalization of gauge-invariant effective actions.

In the lattice QCD the gauge field $A_\mu(x)$ is replaced by a connector operator $U(x, \; \mu)$ defined on the link $[x, \; x + a\,e_\mu]$:

$$U(x, \; \mu) \stackrel{\mathrm{def}}{=} \left( i g \int_x^{x+e_\mu} A_\mu \, \mathrm{d}\,x^\mu \right) \tag{7}$$

where $g$ is the constant of interaction. The same link in the opposite direction describes the inverse of the group element $U$. Lattice plaquettes $U_1 U_2 U_{-1} U_{-2}$ contribute to the functional integral for

an amplitude containing a quark antiquark pair. Each plaquette gives a suppression factor $1/g^2$; a total suppression factor rises to a power equal to the number of plaquettes needed to produce the surface in between

$$\left(1/g^2\right)^\ell = e^{-V(x_1, x_2)} \tag{8}$$

where $\ell$ is the distance between the quark lines; $t$ is the interval in the Euclidean time direction. Matrix elements of the operator $e^{-tH}$ include a potential term $V(x_1, x_2)$ that increases linearly with the distance $\ell$ between the quark lines. This means that the present potential confines the interacting quarks.

A topological phenomenon is associated with the Higgs field potential

$$V(\varphi) = \tfrac{1}{2}\left(\varphi^*\varphi - F^2\right)^2 \tag{9}$$

where $F$ is the vacuum expectation value of the Higgs field $\varphi$. The gauge transformation replaces the $\varphi$ field of a vortex by a field dissolved in the vacuum, which has $\varphi \to F$ everywhere. Such vortexes represent magnetic monopoles and the vortexes possess end points. That is why in this pattern magnetic monopoles are tied together by vortex lines and 't Hooft concludes: "Since a vortex carries energy proportional to its length, one finds that in a Higgs theory, magnetic monopoles are absolutely confined, exactly in the way one expects quarks to be confined in QCD".

A chain of gluons implies that the energy of gluon fields in their environment tend to infinity when the inter-quark distance goes to infinity. A confining potential from the start is chosen in the form of a Coulomb potential, though this requires justification. Further infrared renormalized procedures allows one to derive a Green function that includes a Yukawa potential

$$G(\vec{x} - \vec{x}') = \delta^3(\vec{x} - \vec{x}') - \frac{8\pi\sigma}{\alpha|\vec{x} - \vec{x}'|}\exp(-\sqrt{2\sigma/\alpha}\,|\vec{x} - \vec{x}'|), \tag{10}$$

which exactly shows the confinement.

A renormalization of gauge-invariant effective actions is reduced to the consideration of a flux tube (a "tube" between two quarks in Fig. 1) filled with a field of the energy density, the D-field, where the energy density is defined as $W(D)$ [46]. The vortex with given total flux $Q = D\Sigma$ spreads over a surface $\Sigma$ in such a way that the total energy is minimized. Then the energy per unit of length of this vortex is

$$\rho^{\text{string}} = \min\left(\Sigma\,W(D)\right). \tag{11}$$

The functional on the right hand-side of Eq. (11) has a non-trivial minimum, which is reached at special conditions and can be associated with the confinement.

A supergravity background that produces linear confinement of quarks in four dimensions has recently been presented [47]. El Naschie [48] interprets quarks confinement involving a phase transition of quantum spacetime at the Planck scale at which the confinement is absolute at a certain energy scale limit where the Planck energy is $M_{\text{P}} = 10^{19}$ GeV.

As point out Alkofer and Greensite [45], the confinement problem becomes one of the truly fundamental problems in physics. They mention that quark confinement is the essential link between the microscopic quark-gluon degrees of freedom of QCD, and the actual strong-interaction spectrum of color-neutral mesons, baryons, and nuclei. They conclude as follows: "Until this phenomenon is well understood, something essential is still lacking in our grasp of the foundations of nuclear physics, and the deeper mechanisms of nonabelian gauge theory. Although the confinement problem is hard, the solution is important, and well worth pursuing. But it is certainly not excluded that progress may come from some quite different direction" [45].

# 3. Other views on quarks and hadrons associated with QCD

In the physics of quarks the researchers initially consider the interaction between two quarks, then, as a second step, one introduces a third quark to this diquark system, etc., in order to obtain the

complete wave function of a baryon; this method is a good approximation as long as three-body interactions are rather small compared to two-body interactions [49]. The introduction of three colors for each quark complicate the study, as a diquark system becomes non-distinguished from an antiquark.

Modern experiments [50], first of all scattering experiments of electrons and positrons, provide support for the standard model of six quarks with three colors. The idea of color charge allowed one to explain how quarks could coexist inside some hadrons in otherwise identical quantum states without violating the Pauli exclusion principle. Each flavor of quark belongs to the fundamental representation, $SU(3)$, and contains a triplet of fields $\psi = (\psi_1, \psi_2, \psi_3)$. These three indices are usually identified with the three colors, such that after gauge transformation, the new colors are linear combinations of the old colors. Nevertheless, the standard model of particles allows also an arbitrary number of colors [51].

Moreover, the deep inelastic experiments do not rule out even integer-charge quarks [52-55]: in higher orders of perturbation the integer-charge quark model gives results closer to those of the fractional charge quark model and the properties like factorization of mass singularities, which have been shown for the fractional charge quark model, assume also for the integer-charge quark theory. Rajasekaran and Rindani [52] point out that a clear and unambiguous high-energy test, which distinguishes the one model from the other, has not yet been found: "As long as it leads to almost similar empirical phenomena to that of the fractional-charge quark model, it is going to be very difficult to rule it out experimentally. It may even be the right model! Although exact $SU(3)c$ symmetry appears to be an elegant hypothesis, exact $SU(3)c \times U(1)$ does not look so elegant. Why can't the degenerate gluons and photon mix and break the symmetry?"

Thus in QCD the integer-charge quark is not ruled out, which was shown by conventional field methods [52-55]. Integer charge quark theories (ICQ) fit experimental data far better than the standard model does [54, 55]. In particular, Ferreira [54] have reviewed the evidence for fractional quark charges and argued that they are not conclusive. On the other hand since ICQ theories are renormalizable they demonstrate a good comparison with experiment data, which is held for any order of perturbation theory; ICQ theories also predict identical rates for meson radiative decays. In the end Ferreira [54] states: "Regardless of whether one believes in ICQ models or not, it seems clear they do a better job than the Standard Model at describing the two-photon data."

We will see that violating the Pauli principle is quite possible and even necessary in the dynamics of quarks.

A light-front approach [56] to QCD formulates light-front Hamiltonian as a complementary approach to the well-established lattice gauge method. It is a Hamiltonian method, formulated in Minkowski space rather than Euclidean space. The essential ingredient is Dirac's front form of Hamiltonian dynamics where one quantizes the theory at fixed light-cone time $\tau = t + z/c$ rather than ordinary time $t$. The approach offers access to the hadron's nonperturbative quark and gluon amplitudes that allow testability in experiments.

The Nambu–Jona-Lasinio (NJL) model [7, 8] is considered to be a model for the low-energy regime of QCD. The NJL Model is a non-renormalizable quantum field theoretical model for dynamical chiral symmetry breaking; this model picks chiral symmetry but does not provide a mechanism for confinement and, consequently, the NJL model needs a plausible explanation for this neglect [57]. In the mean-field approximation the Lagrangian density is

$$L = L_0 + \bar{\psi} M \psi \tag{12}$$

where the first term is the conventional Dirac Lagrangian density and the "effective" mass $M$ satisfies a self-consistent equation

$$M = \frac{2GM}{\pi^2} \int_0^\Lambda \frac{p^2 \, dp}{\sqrt{p^2 + M^2}} \tag{13}$$

where $G$ is a parameter with the dimension of square length. Eq. (13) has a non-vanishing solution in the case when $G > G_{\text{critical}}$. For these values of the coupling constant, chiral symmetry is dynamically broken.

The NJL model further describes [58] dynamical quark mass generation and spontaneous chiral symmetry breaking and includes effects of the axial U(1) anomaly; mesons emerge as quark-antiquark modes; the quark-diquark structure of baryons is developed, and a brief summary is given on baryonic solitons as they result from the NJL model. A semi-classical NJL model of an instanton liquid for mesons and quark condensates in which lowest multi-quark interactions dominate look quite reliable [59]. Other aspects of the NJL model were considered in Refs. 59, 60. Quark droplets of finite volume were formulated in the NJL model with a basic set of the quark wave functions in the chiral bag model in work [61]; chiral symmetry breaking for the finite volume bag was discussed in a mean field approximation, effects of the pion cloud including the chiral Casimir effect were investigated, and physical quantities of the quark droplets, such as masses and radii, were obtained for baryon numbers $A \leq 5$.

The Skyrme [9, 10] field theory has static solutions of a singular nature, but finite energy, characterized by spin directions. He introduced an additional term in the field gauge theory, which makes it possible for baryons to interact with each other via the exchange of mesons. Skyrme [10] introduced the Lagrangian

$$L = \frac{f_\pi^2}{4} \text{Tr} \left[ \partial_\mu U \, \partial^\nu U \right] + \frac{1}{32 g^2} \text{Tr} \left[ U \partial_\mu U, \ U \partial_\nu U \right]^2 \tag{14}$$

where the $f_\pi$ is the pion decay constant, $g$ is the constant known as the $\rho$-$\pi$-$\pi$ coupling, the field

$$U = \exp \left\{ i \, \tau \, \cdot \varphi / f_\pi \right\} = \left( \text{s} + i \, \tau \, \cdot \pi \right) / f_\pi, \tag{15}$$

$\tau$ is the vector containing The Pauli matrices, $\pi$ the pion field. The first term in the Lagrangian (14) is the usual nonlinear sigma model; the second part was introduced by Skyrme [10].

Skyrme revealed a family of classical static solutions approximating QCD at low energies, which were called skyrmions. The appropriate equation of motion derived from the Lagrangian (14) has the form

$$U_S = \exp \left\{ i \, \tau \cdot \hat{r} \, F(r) \right\}, \tag{16}$$

where $F(r)$ is a radial function satisfying certain boundary conditions [62].

Topological soliton solutions, or topological charges, minimize the energy and may be identified as the baryon number. The physical interpretation of these solitons is still not quite clear, nevertheless, most recent studies account for skyrmions rather as coherent states of baryons and excited baryons [62]. This model describes hadrons and their interactions without taking their quark content into account. Nevertheless, electromagnetic properties of baryons calculated with the Skyrme model are in agreement with experimental values for a number of baryons [63]; besides, Weigel [63] shows that the NJL model can be employed to involve solitons in a microscopic theory of the quark. One more application of the Skyrmion model is a possibility of Skyrmion (neutron) stars that can be looked at as being made of fermionic soliton objects [64, 65]. It has recently been found [66] that the single soliton in the Skyrne model is composed of $N$ partons that are topologically confined; multi-soliton solutions have been computed and related to polyiamonds, which are plane figures composed of equilateral triangles joined by common edges. It is shown that those solitons may be viewed as pieces of a doubly periodic soliton lattice.

The MIT bag model [11-14] was developed by nuclear physicists and reflects major peculiarities of nuclei. It describes the particles as composite systems with their internal structure that can be associated with quark and gluon field variables. In the model, quarks are forced by an external pressure on the side of a vacuum and are able to move only in a closed spatial region, i.e. a bag, in which quarks occupy single particle orbitals. When all the quarks are in the ground state, the shape of the bag is spherical.

Each quark is described by the Dirac field inside a bag,

$$\left( -i \, \gamma^\mu \frac{\partial}{\partial x^\mu} + m \right) \psi_a(x) = 0. \tag{17}$$

The boundary condition

$$i \, \vec{\gamma} \cdot \vec{n} \, \psi_a = \psi_a \tag{18}$$

7

where $\gamma^\mu$ are the Dirac matrices and $\vec{n}$ is the unit normal vector. $\psi_a(x)$ is discontinuous across the surface of the bag, since $\psi_a(x) = 0$ outside. Eq. (17) allows one to calculate the energy and momentum that flows through the surface. Momentum and energy flow inside the hadron studied are characterized by a stress tensor $T^{\mu\nu}_{\text{Dirac}}(x)$. The total energy and momentum of the hadron should not flow through the surface. The flow is given by $n_\mu T^{\mu\nu}_{\text{Dirac}}$ calculated on the surface; this flow is reduced to the equation

$$ n_\mu T^{\mu\nu}_{\text{Dirac}} = \tfrac{1}{2} \frac{\partial}{\partial x_\nu} \left( \sum_a \bar{\psi}_a(x)\, \psi_a(x) \right). \tag{19} $$

Since $\bar{\psi}_a \psi_a = 0$ on the surface, its derivative lies along the normal,

$$ \frac{\partial}{\partial x^\nu} \left( \sum_a \bar{\psi}_a\, \psi_a \right) = n_\nu\, 2\, P_{\text{Dirac}}. \tag{20} $$

Thus $n_\mu T^{\mu\nu}_{\text{Dirac}} = n_\nu\, P_{\text{Dirac}}$, which allowed the authors [11-14] to recognize $P_{\text{Dirac}}$ as a normal pressure on the surface of the bag. The conservation of energy and momentum within the hadron requires an introduction of the other kind of a pressure to compensate the Dirac pressure $P_{\text{Dirac}}$. Thus, it was postulated that the total energy momentum tensor consists of two parts

$$ T^{\mu\nu}_{\text{hadron}} = \begin{cases} T^{\mu\nu}_{\text{Dirac}} - g^{\mu\nu} B & \text{(inside)} \\ 0 & \text{(outside)} \end{cases} \tag{21} $$

Here, $B$ is a universal constant with the dimension of pressure, $E/V$ (in units of $\hbar = c = 1$, $B^{1/4}$ has the dimension of mass). Thus the balance equation becomes

$$ B = -\tfrac{1}{2} \frac{\partial}{\partial r} \left( \sum_a \bar{\psi}_a \psi_a \right) = P_{\text{Dirac}}. \tag{22} $$

If $P_{\text{Dirac}}$ is produced by the energy and momentum flow inside the hadron, $B$ is a fitting parameter, which has a volumetric nature and can be interpreted as the pressure of an outside vacuum on the whole bag (or more exactly, the bag surface).

Eqs. (17), (18) and (22) can be solved for the spherical shape ($r = R$) and in the ultrarelativistic limit ($m \to 0$). In this case the quarks occupy the lowest mode with frequency $\omega = 2.04/R$. Then the energy of the hadron is directly derived from the equation

$$ P^0 = E = \int d^3x \left( T^{00}_{\text{Dirac}} + B \right), \tag{23} $$

such that

$$ E_n = n \frac{2.04}{R} + \frac{4\pi}{3} B R^3 \tag{24} $$

where $n$ is the number of quarks in the hadron. The first term in expression (24) is usual in quantum mechanics; it represents discrete energy eigenvalues, i.e. the term depicts the kinetic energy of the quarks that occupied the lowest orbital. The second term in expression (24) expresses the stabilizing potential energy that results form the external pressure. Thus the introduction of a phenomenological parameter $B$ could guarantee the implementation of the boundary condition.

Minimizing Eq. (24) with respect to $R$ makes it possible to obtain expressions for the radius of the hadron and its energy as a function of the parameter $B$ and the number $n$ of quarks:

$$ R_n = [2.04\ n/(4\pi B)]^{1/4}, \quad E_n = \tfrac{4}{3}\ (4\pi B)^{1/4}\ (2.04\ n)^{3/4} \tag{25} $$

Introducing $m \neq 0$, the angular momentum and the interaction with color gluons complicate the problem. The bag model was further developed by many researchers (see, e.g. Refs. 67-71). In particular, in the book [72] the chiral bag model was considered as a hybrid model of the MIT
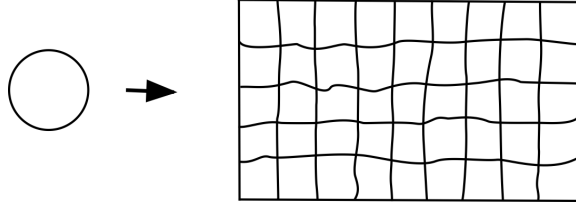
8

Figure 2: Topological ball and the tessellattice formed of such balls.

bag model and the Skyrme model, which allowed a solution in a special configuration called the hedgehog ansatz for a solitonic solution for the nucleon.

A review [73] on topological soliton models discloses the foundation of the approach and the application of topology to classical field theory; the main accent is on a property called homotopy, which describes how two maps (such as two different field configurations) can (or cannot) be continuously deformed into each other. In the context of physics, this deformation is often interpreted as the time evolution of the system. Baryons allow description in chiral topological soliton models in which they appear as topological excitations of an effective action that depends only on the chiral field $U(\mathrm{x})$. The study is based first on the Skyrme action (with an addition of some others) [74, 75]. In the soliton picture the strong interaction properties are used; baryons are computed following the $SU(3)$ collective coordinate approach to the Skyrme model. In paper [75] hyperon masses were described in the topological soliton model; these masses are very sensitive to parameters of the gluon condensate, which contrasts with the insensitivity of the soliton properties to coupling of quarks and gluons though a hypothetical particle 'dilaton'. The bag formed by the scalar field dynamically and emerged as very shallow.

On the other hand, a very popular approach also based on a non-topological soliton, which represents a field configuration possessing, contrary to a topological one, a conserved Noether charge and stable against transformation into usual particles of this field [76]. The mass sum of free particles with the charge $Q$ exceeds the total energy of the non-topological soliton so that the soliton becomes energetically favorable to exist.

# 4. Leptons and quarks in the tessellattice

A detailed mathematical theory of the real physical space based on topology, set theory and fractal geometry, was developed in works [16-19]. It was shown that the space is not a vague vacuum, but a substrate arranged as a mathematical lattice of primary topological balls (Fig. 2). This lattice was called a tessellattice; it was postulated that the size of a cell is equal to the Planck length $\sqrt{\hbar G/c^3} \cong 1.616 \times 10^{-35}$ m.

In the tessellattice balls are found in a tight state, which corresponds to a degenerate state of the real space. This space holds for a quantum void since on one hand, it provides a discrete topology, with quantum scales, and on the other hand it contains no "solid" object that would stand for a given provision of physical matter. The appearance of a stable local deformation is possible when a transformation of a cell involves some iterated internal similarity. Then the appropriate cell becomes a particable ball, which thus is represented by a nonhomeomorphic transformation in a continuous deformation of space elementary cells.

Since we have introduced a particle in the tessellattice, we must provide it with physical properties. First of all this is mass: The mass $m_A$ of a particulate ball $A$ is a function of the fractal-related decrease of the volume of the ball:

$$m_A \propto (\mathcal{V}^{\mathrm{deg.\ cell}}/\mathcal{V}^{\mathrm{part}}) \cdot (\mathrm{e_{fract}} - 1)_{\mathrm{e_{fract}} > 1} \tag{26}$$

where $\mathcal{V}^{\mathrm{deg.\ cell}}$ is the typical average volume of a cell in the tessellattice in the degenerate state; $\mathcal{V}^{\mathrm{part}}$ is the volume of the kernel cell of the particle; (e) is the Bouligand exponent, and $(\mathrm{e_{fract}} - 1)$

9

the gain in dimensionality given by the fractal iteration (just a volume decrease is not sufficient for providing a ball with mass, since a dimensional increase is a necessary condition; there should be a change in volumetric fractality of the ball [17, 18]).

Therefore mass appears as a deformation of a cell, i.e. at the volumetric fractal contraction of the cell. This is typical for leptons, namely, $\mathcal{V}^{\text{deg. cell}}/\mathcal{V}^{\text{lepton}} > 1$ determines the lepton's mass (26).

In the tessellattice a lepton is a contracted kernel-cell (Fig. 3a). Surrounding cells compensate this local deformation by morphic changes; namely, they move from the initial equilibrium positions and are stretched, experiencing a certain tension (rather a radial tension) compared to cells in the degenerate sate. These surrounding stretched cells form a peculiar deformation coat with a radius identified with the particle's Compton wavelength $\lambda_{\text{Com, lept}} = h/(m_{0,\text{lept}}c)$ (note this radius manifests itself through the experiments on light scattering by particles). It seems the contracted kernel-cell is unstable to radial standing oscillations that spread the deformation $\mathcal{V}^{\text{deg. cell}}/\mathcal{V}^{\text{lepton}}$, i.e. the proper lepton's mass $m_0$, throughout the whole deformation coat [23]: the mass $m_0$ decays in the deformation coat such that its pieces are dancing in the deformation coat hopping from cell to cell from the kernel-cell and back.

In the case of quarks the situation is reciprocal: the quark's kernel cell has volume bigger than the average volume of a degenerate cell, i.e. $\mathcal{V}^{\text{quark}}/\mathcal{V}^{\text{deg. cell}} > 1$ [17, 18]. Quarks are inflated objects (Fig. 3b).

Since the notion of mass is associated with the decrease of volume of a cell, quarks definitely do not possess mass as such, which is in agreement with requirements of QCD [77, 78]; quarks can be described in terms of energy. Quarks manifest themselves through the unification, which produces matter - mesons, protons, neutrons, etc. That is why a deformation coat of contracted (i.e. massive) cells around unified quarks must exist as well. Thus the mass comes to the quark through its deformation coat in which cells are contracted, i.e. are massive.

Due to the inflated kernel-cell, cells around the quark's kernel-cell move apart from their equilibrium positions. These moved cells should be a little bit contracted in the framework of the quark's Compton wavelength $\lambda_{\text{Com, quark}}$ and the total sum of contracted cells has to compensate the inflation of the kernel-cell. Hence in the quark's deformation coat contracted cells around the kernel-cell represent the quark's total mass $m_{0,\text{quark}}$ (see the definition (26)) and this mass defines the value of the quark's Compton wavelength $\lambda_{\text{Com, quark}} = h/(m_{0,\text{quark}}c)$. It is reasonable to assume that the inflated kernel-cell is unstable to radial standing oscillations, as is the case for a lepton. At such oscillations, bits of the inflated state of the kernel-cell spread all over all other cells of the quark's deformation coat. This means that the quark's deformation coat filled with volumetric inflated excitations can be treated as a bubble.

A different fractional volume of the appropriate kernel-cell characterizes a set of leptons, i.e. the more massive lepton, the smaller the characteristic radius of the appropriate kernel-cell. In the case of quarks the situation is opposite: the larger the radius of the kernel-cell, the heavier the quark.

## 4.1 The behavior of leptons

In the case of leptons it has been shown [23] that the deformation coat formed around the particle participates in a common oscillation process of all cells of the coat. This process is described by a single vibration mode. Further studies [27] showed oscillations of cells in the deformation coat obey a standing spherical wave, i.e. the amplitude of oscillation of mass is inversely proportional to the distance from the central point, $m \propto 1/r$.

The motion of a lepton in the tessellattice was studied in works [20-24]. The developed submicroscopic mechanics is specified with the interaction with space, i.e. the tessellattice. As a result, we arrived at the de Broglie's relationships for a particle

$$E = h\nu, \qquad \lambda = h/(mv), \tag{27}$$

which in fact demonstrates a discrete structure of space, because $\lambda$ plays the role of a spatial period of the particle: each odd section $\lambda/2$ the particle emits excitations (due to the interaction
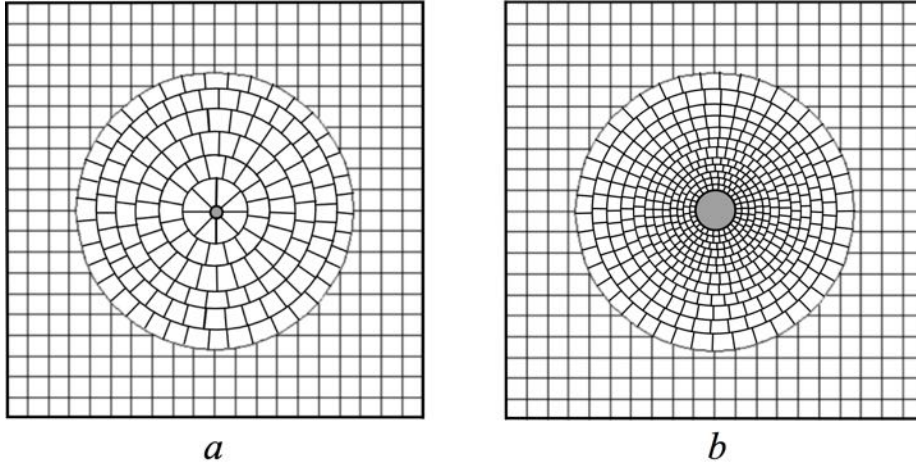
Figure 3: Lepton ($a$) and quark ($b$) in the tessellattice. Each lepton is specified by its own quantum size of the kernel cell and the same for quarks. The leptons kernel cell ($a$) is less than a degenerate cell of the tessellattice; in the deformation coat around the kernel's lepton-cell cells are stretched, they have a certain tension (radially "inflated") compared to cells in the degenerate sate. The quarks kernel cell ($b$) is larger than a degenerate cell of the tessellattice and one can anticipate a few quantum sizes; in the deformation coat around the kernel's quark-cell cells are compressed (radially "contracted") compared to cells in the degraded state. The size of the deformation coat is defined by the Compton wavelength $\lambda_{\mathrm{Com}} = h/(mc)$. For the electron: $\lambda_{\mathrm{Com\,el.}} = 3.77 \times 10^{-13}$ m; for the light quarks u and d: $\lambda_{\mathrm{Com\,u,\,d}} \approx 3.77 \times 10^{-14}$ m.

with space) and then each even section $\lambda/2$ it absorbs them back. Relationships (27) allow the derivation of the Schrödinger equation, as was shown by de Broglie [79]. Excitations emitted by the particle were named inertons. Submicroscopic mechanics enables us to determine a shape of the 'particle-inerton cloud' system: the inerton cloud is extended to the distance $\lambda$ along the particle's path and to the distance

$$\Lambda = \lambda \, c/\upsilon \tag{28}$$

in transversal directions. Hence we know that the shape of the system in question resembles a spindle and we know its size.

The motion of such extended particle looks like the motion of a liquid particle in a continuum. The equilibrium state of volumetric fractals, which introduce deformations in cells of the liquid particle, is related to the value of mass and therefore determines a density $\rho$ of this liquid particle. In the process of motion these deformations (volumetric fractals) in the appropriate cells have to tense, which will produce a displacement vector $\vec{\xi}$ for our liquid particle. For the description of such moving liquid particle we may employ the known results of field theories used in hydrodynamics. Indeed, we may begin with the Lagrangian density (see, e.g. Ref. 80)

$$L = \tfrac{1}{2} \, (\dot{\vec{\xi}} \cdot \dot{\vec{\xi}}) \, - \, \tfrac{1}{2} \, \upsilon^2 (\nabla \cdot \vec{\xi})^2 \tag{29}$$

where $\vec{\xi}$ is the displacement vector, or tension of our continuous system in the place occupied by the liquid particle studied; $\upsilon$ is the velocity of the liquid particle. Matter is available only in a volume $\mathcal{V}$ of the space occupied by the particle; let the matter be characterized by the density $\rho$ and let $\rho_0$ be its initial, or equilibrium value. Then the continuity equation is

$$\dot{\rho} \; + \; \rho_0 \, (\nabla \cdot \dot{\vec{\xi}}) = 0. \tag{30}$$

The Euler-Lagrange equations constructed on the basis of the Lagrangian density (29) and Eq. (30) culminate in equations

$$\ddot{\vec{\xi}} \, - \, \upsilon^2 \, \nabla \cdot (\nabla \cdot \vec{\xi}) = 0, \tag{31}$$

$$\Delta \rho - \ddot{\rho}/\upsilon^2 = 0. \tag{32}$$

The most interesting is Eq. (32) that describes the propagation of density of the {particle-inerton cloud} system; it takes the form of the wave equation for sound waves. The solution to Eq. (32) can be searched proportional to $|\cos(4\pi \, \nu \, t)|$, which results in

$$\Delta \rho \; - \; \frac{16 \, \pi^2}{\lambda^2} \rho = 0 \tag{33}$$

where we use the correlation $\nu = \upsilon/\lambda$; here $\nu$ is the frequency of the wave, $\lambda$ is the wavelength and $\upsilon$ is the sound velocity. Note that the role of the frequency $\nu$ of this peculiar sound wave plays the frequency of collision $1/(2T)$ of the moving particulate cell (the particle kernel, Fig. 1) with its inerton cloud [20-23].

Eq. (33) can be modernized by using the second relation in de Broglie's relationships (27)

$$\Delta \rho - \frac{16 \, \pi^2 m^2 \upsilon^2}{h^2} \rho = 0. \tag{34}$$

Then utilizing the energy conservation law for our moving particle

$$E = m\upsilon^2/2 \; + \; V \tag{35}$$

where $V$ is a potential energy, we finally obtain instead of Eq. (33) an equation

$$\Delta \rho \; - \; \frac{2m}{\hbar^2}(E - V)\rho = 0, \tag{36}$$

which appears as the Schrödinger wave equation, but the role of the wave $\psi$-function is played by the density $\rho$ of the {particle + inerton could}-system; since the $\psi$-function is dimensionless, the
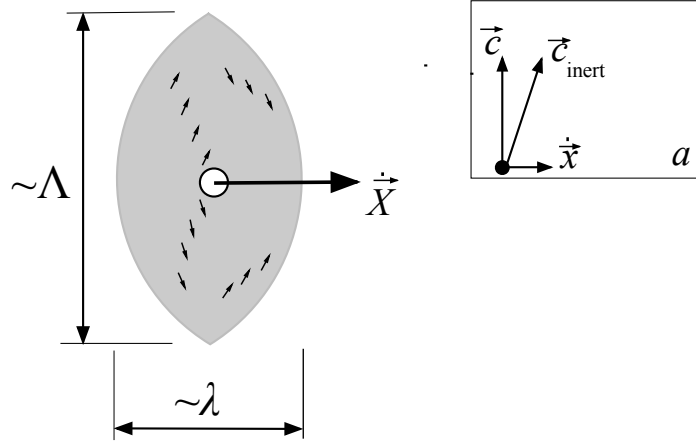
12

Figure 4: Particle moving together with its inerton cloud in the real space. The $\psi$-wave function is a project of the {particle + inerton cloud}- system to an abstract phase space. The particle moves squeezing in between cell, though the state of deformation coat adjusts to the particle in any point of the particle's path. Inertons migrate hopping from cells to cells like excitons in molecular crystals.

normalized function $\rho/\rho_0$ should exactly correspond to it. Note in Eq. (36) in the function $\rho$ the value of the mass field varies (rather than the volume $V$), however, in the second term the value of the parameter $m$ must remain fixed ($m$ represents the initial value of mass, i.e. the particle's inert mass $m = m_0/\sqrt{1 - v^2/c^2}$). A complex part of $\rho$ means that the appropriate part of the particle's mass is transferred to a tension of the surrounding space.

Thus we return a physical sense (Fig. 4) to the wave $\psi$-function, whose module so far was interpreted as a probability of the particle location after Max Born since 1926 [81, 82]. The physical pattern looks as follows: a moving particle is surrounded with a cloud of excitations (named *inertons* in the author's works), which exactly corresponds to the electron described by Poincaré [83], who hypothesized that the moving electron should create a cloud of excitations in the ether. De Broglie's relationships (27) bound the particle's parameters $E$ and $p$ with parameters of the particle's excitations – the section $\lambda$ (the de Broglie wavelength that can be called an amplitude of the particle) in which the particle's velocity decreases to zero and then increases to the initial value $v$ again, and the frequency $\nu$ of collisions of the particle with its cloud of inertons. Relationship (28) connects the amplitude $\Lambda$ of the inerton cloud with the particle's amplitude $\lambda$, the speed $c$ of the cloud's inertons and the speed $v$ of the particle.

In special relativity a vacuum is invariant under a Lorentz transformation and this transformation influences space that undergoes a Lorentz contraction. In the case of the tessellattice, which substitutes a vague vacuum, the Lorentz contraction is passing on to the moving object, i.e. the object itself experiences the Lorentz contraction. How this happens has been shown in Ref. 17: the hidden structure of the initial Lagrangian

$$L = -m_0 c^2 \sqrt{1 - v^2/c^2} \tag{37}$$

emerges owing to the introduction of the interaction of the moving particle with space (i.e. the tessellattice)

$$L = -m_0 c^2 \sqrt{1 - \frac{1}{m_0 c^2} \left\{ m_0 \dot{x}^2 + m_0^{(\text{in})} \dot{x}^{(\text{in}) \, 2} - \frac{2\pi}{T} \sqrt{m_0 m_0^{(\text{in})}} \left( x \dot{x}^{(\text{in})} + v_0 x^{(\text{in})} \right) \right\}} \tag{38}$$

In expression (37) there is a process, which is hidden inside the expression: the moving particle emits its inerton cloud (due to the friction with space) and hence we have two objects that travel
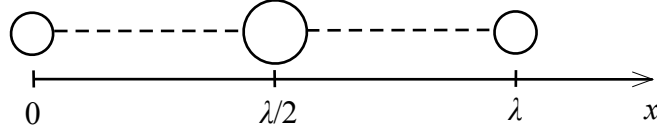
13

Figure 5: Particle radius oscillates along the de Broglie wavelength $\lambda$.

together: the particle (mass $m_0$) and its inerton cloud (mass $m_0^{(\text{in})}$). The motion is specified with the interaction $\sqrt{m_0 m_0^{(\text{in})}}$ that takes place in the time interval $T$, which becomes the time of collisions (and $T^{-1}$ is the frequency of collisions). All this occurs in the section equal to the particle's de Broglie wavelength $\lambda$. The described inner kinetics is presented in the Lagrangian (38). If the path of the particle is much longer than $\lambda$ and the scale is rather close to macroscopic, we may revert back to the classical consideration (37). The Euler-Lagrange equations obtained on the basis of the Lagrangian (38) allow the study of the system {particle + inerton cloud} in detail [21-24].

High-energy physics is expressed in a relativistic form. The energy expression (35) takes a Newtonian form. In papers [17, 21-24] it is shown that owing to the transformation of the relativistic Lagrangian (37) to the form (38), the kinetic energy of a very fast particle ($v \to c$) emerges as follows

$$E = \tfrac{1}{2} m \dot{x}^2, \qquad m = m_0/\sqrt{1 - v^2/c^2}, \tag{39}$$

though the total energy is still

$$E_{\text{total}} = m c^2, \qquad m = m_0/\sqrt{1 - v^2/c^2}, \tag{40}$$

where at the approximation $v \to c$ the kinetic energy (39) is approaching to the total energy (40). Therefore, all is correct when applying expression (35) to high-energy physics.

Let us list the main important properties of leptons revealed in the framework of submicroscopic mechanics developed in the tessellattice.

The kernel-cell representing the particle changes along a particle's path as Figure 5 depicts. Thus spin-1/2 is a dynamic characteristic, which can be associated with periodical oscillations of the surface state of the particle's kernel-cell (electron, muon, $\tau$-lepton) along the particle's path [22, 23]: a mobile state (when it possesses the velocity in even points of the de Broglie wavelength $\lambda/2 \cdot l$ where $l = 0, 2, 4, ...$) changing to a stationary state (when the needles though are bended, but immobile in the odd points of the de Broglie wavelength $\lambda/2 \cdot l$ where $l = 1, 3, 5, ...$). The integer spin would belong to particles combined of two Fermi particles. Nevertheless in the case of a photon the spin-1 is only words ? no any inner physical behavior for this quasi-particle (the electromagnetic field particle) can be suggested. The phrase: ?photons obey the Bose-Einstein statistics? means only that they are quasi-particles without spin-1/2 whose states change discretely. In the case of cold diluted gases that form a Bose-Einstein condensate, the situation is not associated with the value of spin as well: each atom irradiates its proper inerton cloud that then is completely absorbed by the neighbor atom [24]. It seems the Bose-Einstein statistics describes quantum particles/quasi-particles that do not have spin at all.

The value of mass $m$, a total fractal volumetric deformation of the particable cell, oscillates along the section $\lambda$ as well: the mass $m$ periodically changes from $m$ to 0 and then again to $m$ (Fig. 5), though the tension of the particle varies from 0 to $\xi$ and again to 0 [28].

The electric charge is the state of the kernel particle associated with its surface [26]: a positively changed particle has the surface of a typical chestnut – amplitudes outside; a negatively charged particle has the surface on which surface amplitudes are oriented inside the appropriate topological ball. The value of charge $e$ oscillates along the section $\lambda$ as well: the charge periodically changes from $e$ to 0 (in even points $\lambda/2 \cdot l$, where $l = 0, 2, 4, ...$), though the tension electric state, which corresponds to the magnetic monopole state of the particle, varies from 0 to g (in odd points $\lambda/2 \cdot l$, where $l = 1, 3, 5, ...$), see Fig. 6.
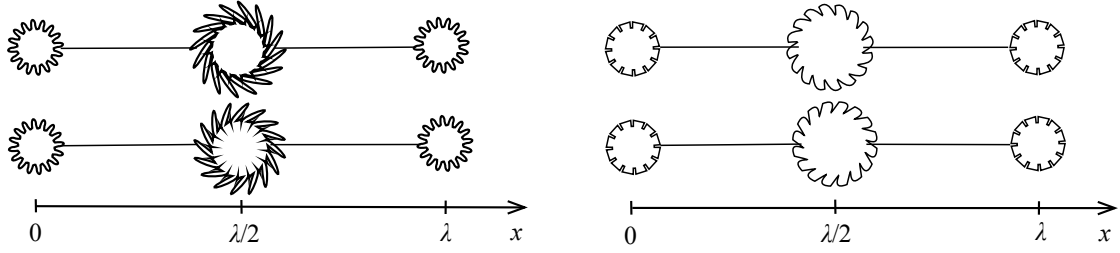
14

Figure 6: Motion of the electrically changed particle: positive (left) and negative (right). The elementary charge periodically changes to the magnetic monopole state (in odd points $\lambda/2 \cdot l$ of the path, where $l = 1, 3, 5, ...$); two possible magnetic polarizations (right and left) are shown. So the charged particle is a dyon (it possesses both electric and magnetic charges).

The photon and the inerton are shown in Fig. 7 (more amply read in papers [25, 26, 28]). These neutral quasi-particles (though the photon is electromagnetically polarized) migrate by a relay mechanism hopping from cell to cell in the tessellattice.

## 4.2 The behavior of quarks

An important provision of the submicroscopic concept stated in the previous subsection is the interaction of a moving particle with the space that is a substrate constituted in the form of the tessellattice. Such an interaction must be presented in the case of a moving quark as well. Thus the interaction with the tessellattice has to introduce some nonlinearity in the behavior of quarks.

As seen from Fig. 3$b$ the quark is in fact a bubble in the tessellattice. It is reasonable to assume that by analogy with leptons, its kernel cell constantly exchanges with the quark's coat by excitations: the inflated state periodically decomposes and inflated excitations spread and oscillate in the medium of compressed (massive) cells of the quark's deformation coat. Due to the central symmetry, such oscillations of inflated excitations can be compared to oscillations of a gas in a real bubble, in which the gas oscillations obey the inverse law, $\propto 1/r$. Hence the vibration energy of the quark

$$E_{\mathrm{vib}} \propto 1/r. \tag{41}$$

These excitations are 'inflated inertons', or 'inverse inertons'; below we will name them *qinertons* (quark-inertons).

The naked quark (Fig. 3$b$) is unstable and collapses under the pressure of the whole space. But interacting with another partner(s) they jointly form a stable hadron. The nature of quark confinement is visualized with the use of an elastic bag (bubble) that allows the quarks to move around freely; the bag-bubble is stabilized against the pressure of the confined hadron constituent fields by vacuum pressure and surface tension [67].

Let two bubbles interact (see, e.g. Ref. 84), which means that their surfaces overlap forming a structure shown in Figure 8. In the place of touching the bubbles make a channel with a cross-section $\pi \varepsilon^2$. Disappearance of two borders between the bubbles in a local place means that the energy of the bubbles decreases to the value of $\Delta E = -2\gamma \pi \varepsilon^2$ where $\gamma$ is the coefficient of the surface tension of the bubble. If we put $2\chi << 2R$, where $R$ is the radius of the bubble and $\chi$ is the range of overlapping of the bubbles, this will mean that the total fusion of the bubbles does not occur. Then from the equality $R^2 = \varepsilon^2 + (R - \chi)^2$ we get $\varepsilon^2 \cong 2R\chi$. Hence the energy of attraction of two bubbles becomes

$$\Delta E_{\mathrm{att.}} = -2\,\pi\,\gamma\chi \cdot (2R - \chi) \approx -4\pi\gamma\chi R \tag{42}$$
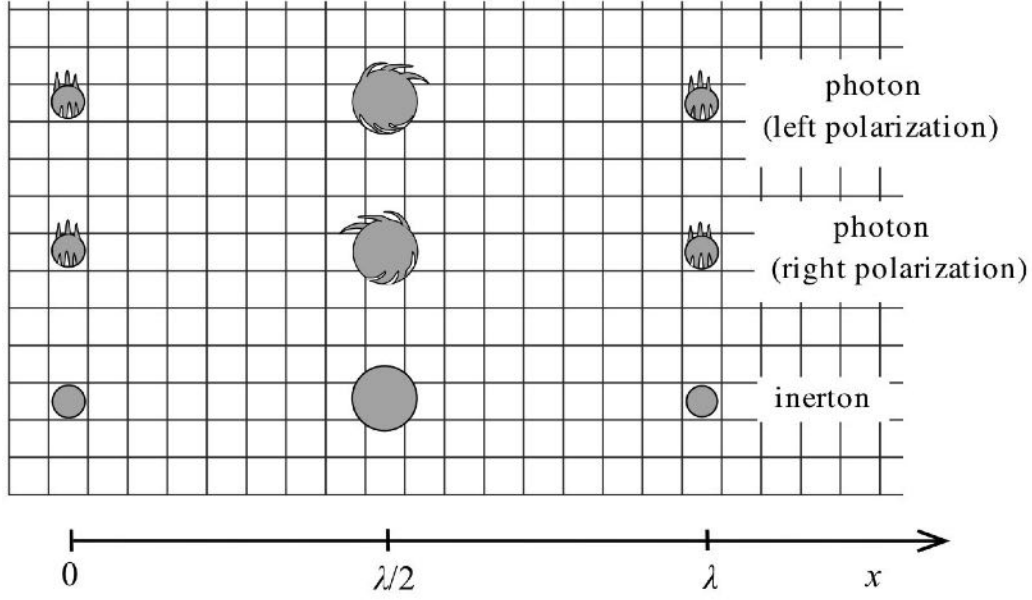
15

Figure 7: Motion of two field particles: the photon and the inerton, which are basic quasi-particles of the tessellattice. The photon's polarization periodically changes between electric (in even points of its path, $\lambda/2 \cdot l$, where $l = 0, 2, 4, ...$) and magnetic (in odd points of its path, $\lambda/2 \cdot l$, where $l = 1, 3, 5, ...$).

and $R$ is the radius of the quark's bubble (which can be associated with the quark's Compton wavelength). In Eq. (42) substituting $R$ by $r$ (the distance between the quarks) and putting for the coefficient $4\pi\gamma\chi = \sigma$, we obtain

$$\Delta E_{\text{att.}} = -\sigma r. \tag{43}$$

Combing Eqs. (43) and (41) we arrive at the static quark potential (6), which we will discuss in detail below in section 4.3.

So expressions (43) and (41) result in the static quark potential (6). Thus the confinement, i.e. a linear dependence of the interaction energy of quarks on a distance $r$, is quite natural and derived from the geometry of the contact of two quarks solvated with the quark's proper excitations named qinertons. The interaction proportional $1/r$ is caused by the emission of standing spherical waves of qinertons by a quark in the quark's bubble. This is shown in Fig. 9.

Each quark experiences an outside compression pressure

$$\mathcal{P}_{\text{compr}} = \mathcal{P}_0 + 2\gamma/R \tag{44}$$

on the side of the tessellattice and the bubble surface.

Let us consider a full merge of bubbles. Let $N$ be the number of cells contained in the bubble. qinertons migrate through these cells and these excitations can be treated as analogous of gaseous molecules in a soap bubble. Therefore we may associate the number $N$ of these excitations in the bubble with its volume $4\pi R^3/3$, the pressure $\mathcal{P}$ produced by these excitations and the temperature $\Theta$:

$$\mathcal{P}\, 4\pi R^3/3 = N k_{\text{B}}\Theta \tag{45}$$

where $k_{\text{B}}$ is the Boltzmann constant. From Eq. (45) we get the pressure in the bubble $\mathcal{P} = 3N k_{\text{B}}\Theta/(4\pi R^3)$. The equality of the compressing $\mathcal{P}_{\text{compr}}$ and the stretching $\mathcal{P}$ pressure allows us to derive the number of qinertons $N$ via other parameters:

$$N = \frac{4\pi R^3}{3\, k_{\text{B}}\Theta}\left(\mathcal{P}_0 + \frac{2\gamma}{R}\right). \tag{46}$$
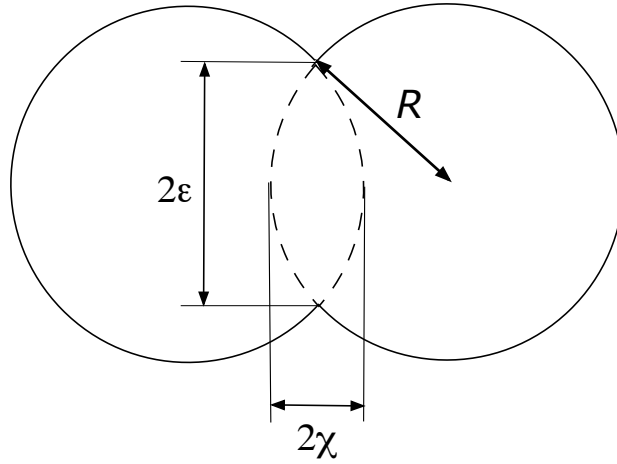
16

Figure 8: Agglutination of two bubbles with quarks located at the bubbles' centers.
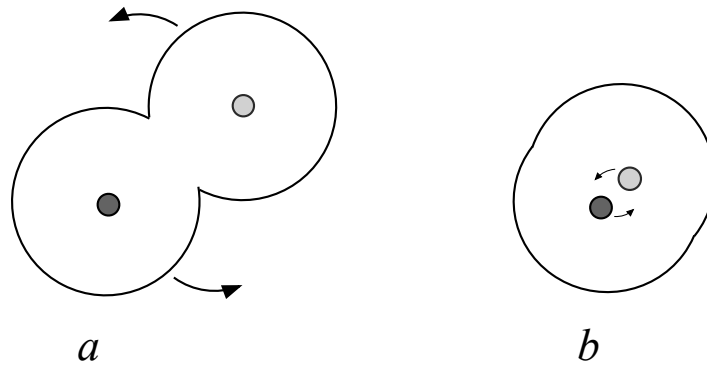


*a*                                        *b*

Figure 9: Confinement of quarks (which is explained in Fig. 8) when they interact with the static potential $V(r) \propto r$ (*a*); free quarks when they interact with a static potential $V(r) \propto 1/r$ (*b*).

The merger of $n$ bubbles is an efficient process. The number of qinertons in a resultant bubble with a radius $\mathcal{R}$ is $\aleph = nN$, which allows us to derive an equation

$$\frac{2\,\gamma}{\mathcal{P}_0} = \frac{n\,R^3 - \mathcal{R}^3}{\mathcal{R}^2 - n\,R^2}. \tag{47}$$

In order to decrease the energy of the bubbles merged together, i.e., reduce pressure on them on the side of the surface and the tessellattice, it is necessary that the numerator and the denominator in Eq. (47) are negative; this is possible when the following inequalities are held (see Ref. 84, p. 37):

$$\mathcal{R}^3 > n R^3, \quad \mathcal{R}^2 < n R^2. \tag{48}$$

Applying inequalities (48) to the problem of quarks, we obtain for the meson and the nucleon, respectively:

$$2^{1/3} < \mathcal{R}/R < 2^{1/2}, \qquad 3^{1/3} < \mathcal{R}/R < 3^{1/2}. \tag{49}$$

Therefore, the united bubble is characterized by a lower Young-Laplace pressure on the quark, $2\gamma/\mathcal{R} < 2\gamma/R$.

Besides, the agglutination of the bubbles allows the quarks to gain an angular motion, which seems to become the major stabilizing factor for existence of the bubbles in the agglutinated state. Indeed, a pair of the agglutinated bubbles, which is extremely quickly rotated, exhibits the integral of the moment of momentum $J \neq 0$. Such a characteristic is lacking for a single quarkable ball in the tessellattice in which a ball (a cell of the tessellattice) is deprived of the opportunity to rotate. That is why the compressing pressure $\mathcal{P}_{\mathrm{compr}}$ at which outside balls of the tessellattice attack the rotating quarks' bubble does not have enough power to collapse the bubble. The equivalent of the sound velocity for the tessellattice is the velocity of light $c$; hence with this velocity surrounding balls attack the bubbles. The energy of hadrons is hundreds of MeV, which means that the velocity of rotating quarks in them $v_{\mathrm{quark}} \approx 0.997\,c$. These two velocities are very close to each other and, therefore, only the vortex state of the quarks can keep the bubbles from collapsing.

As we mentioned above, studying the quark systems, researchers initially consider the interaction between two quarks, then add a third quake, four, etc., which is needed to arrange a wave function of the baryon studied. Quarks are treated as points or rather pseudo-points. The main task is the calculation of the eigenvalue and the binding energy of quarks. But at such an approach diquark system becomes non-distinguished from an antiquark.

The idea of diquark and the achievements of submicroscopic mechanics in the realm of leptons allow us to reconsider the approach to the interaction of quarks. Indeed, the submicroscopic consideration of electrodynamics shows that magnetic monopoles are real entities [26] (Fig. 6), though they are hidden in the inner points of the path of a charged particle. In other words, the moving charged particle periodically changes its charge state to the monopole state. The surface structure of quarks should be the same as in the case of leptons, i.e. needles directed inside (the negative charge) or outside (the positive charge). The combed needles correspond to the magnetic monopole state.

The motion of quarks (Fig. 9) should also obey submicroscopic mechanics, as described above for the case of leptons, because the quark is surrounded with its qinertons and its motion occurs in the tessellattice, which all together is the quark's wave function. This cloud as a whole can be associated with a gluon of QCD. The qinertons also carry electromagnetic properties, as the quark is a charged particle. So, the electrodynamics of a quark is the same as for the electron and positron (Figs. 6, and 7). This means that the electric charge of quarks is integer: $\pm e$ (neither $\pm 2e/3$ nor $\pm e/3$). Below we put for the quark u the charge $+e$, for the quark d the charge $-e$. The antiquark $\bar{\mathrm{u}}$ has the charge $-e$ and the antiquark $\bar{\mathrm{d}}$ has the charge $+e$.

Then the structure for the lightest $\pi$-mesons can be presented as follows:

$$\pi^0 = \mathrm{d\,u}, \quad \pi^+ = \mathrm{u\,g_d}, \quad \pi^- = \bar{\mathrm{u}}\,\mathrm{g_{\bar{d}}} \tag{50}$$

where $\mathrm{g_d}$ and $\mathrm{g_{\bar{d}}}$ are magnetic monopoles of the quark d and antiquark $\bar{\mathrm{d}}$, respectively. Inside of the $\pi^{\pm}$-meson the magnetic monopoles $\mathrm{g_d}$ and $\mathrm{g_{\bar{d}}}$ rotate emitting their own qinertons and

exchanging with similar excitations of the quarks u and ū, respectively. In such presentation the $\pi^-$-meson is the antiparticle to the $\pi^+$-meson and hence their masses are the same. Formulas (50) give automatically known transformations of quarks to leptons (i.e. a bubble collapses to a local deformation, from Fig. 3$b$ to Fig. 3$a$):

$$\pi^+ \to (\text{u}) + (\text{g}_\text{d}) \to \left\{ \begin{array}{l} e^+ + \nu_e \\ \mu^+ + \nu_\mu \end{array} \right. , \quad \pi^- \to (\bar{\text{u}}) + (\text{g}_{\bar{\text{d}}}) \to \left\{ \begin{array}{l} e^- + \bar{\nu}_e \\ \mu^- + \bar{\nu}_\mu \end{array} \right. , \quad (51)$$

i.e., two pairs of the quark and antiquark: u and $\text{g}_\text{d}$, and ū and $\text{g}_{\bar{\text{d}}}$, disintegrate and the quarks and the antiquarks collapse, i.e. they mutate to leptons (51).

In the Standard Model isospin arguments indicate that the $\pi^0$ state is $(\text{u}\bar{\text{u}} - \text{d}\bar{\text{d}})/\sqrt{2}$. However, what does this mixed state of u$\bar{\text{u}}$ and d$\bar{\text{d}}$ really mean with the addition of the factor of $1/\sqrt{2}$? This state shows a mix of wave $\psi$-functions of the corresponding quarks. What do those wave $\psi$-functions mean in the formula $(\text{u}\bar{\text{u}} - \text{d}\bar{\text{d}})/\sqrt{2}$? What is the kinetics of quarks inside the meson? That is, how do the quarks and antiquarks move inside of the $\pi^0$-meson that is characterized by such formula? It is not possible to imagine. The formula $(\text{u}\bar{\text{u}} - \text{d}\bar{\text{d}})/\sqrt{2}$ is rather an abstract writing to satisfy some abstract formalism.

However, as has been shown above, the wave $\psi$-function in the Schrödinger equation (35) is the real thing associated with the central particle and its cloud of excitations. In the case of the present approach the quarks inside of the $\pi^0$-meson are moving by known trajectories (see below the section 4.3). That is why the simple structure of $\pi^0$-meson presented in expression (50) is plausible. Indeed, the pion is neutral and can annihilate by the scheme

$$\pi^0 \to (\text{d}) + (\text{u}) \to \left\{ \begin{array}{l} \gamma + \gamma \\ e^- + e^+ + \gamma \end{array} \right. . \quad (52)$$

Although experimental studies [85] of the decay of $\pi^0$ were carried out in detail, they did not disclose an inner structure of this subatomic particle; the major issues that allowed the examination were the conditions at which the pion appeared and the accurate measurement of its lifetime.

The structure of quarks in the Standard Model is described by unitary symmetry $SU(3)$. Account of the Fermi-Dirac statistics for quarks leads to a splitting of each flavor in three colors, which brings the strong interaction to QCD that operates with color charges exchanging color gluons.

The earlier $SU(6)$ theory [86, 87] successfully explained many experimental facts, but later was rejected because it was thought that from the fundamental point of view, $SU(6)$ was contradictory. $SU(6)$ theory assumes that quarks obey the Fermi-Dirac statistics, but in reality it looks as if they obey the Bose-Einstein statistics.

This paradox was explained by Nambu [88] on the example of the $\Omega^-$ baryon. Its spin is $3/2$, and the strangeness $-3$, so it occupies a state in which the spins of all three S-quarks are parallel. However this state is symmetric under permutation of any pair of particles, in contradiction with the requirement of the Fermi-Dirac statistics. But if for this situation one applies the Bose-Einstein statistics, then for the $\Omega^-$ particle (as well as for other baryons) the values derived by using the $SU(6)$ become consistent with experimental data. So, it turns out that in baryons quarks behave as bosons, but the quarks are separated. Thus, it was recognized that the theory of $SU(6)$ connects the properties that are mutually exclusive and therefore it is too unrealistic.

However, in terms of the proposed deterministic submicroscopic theory this imperfection of the $SU(6)$ theory becomes its advantage. In fact, in our model quarks obey the Fermi-Dirac statistics. However, in hadrons quarks are ultrarelativistic and hence their clouds of excitations are small and do not overlap.

The absence of overlapping clouds immediately prevents the Pauli exclusion principle. The cloud irradiated by one quark is absorbed by another quark. The situation is similar to the behavior of dilute gases of atoms under laser cooling, when a moving atom irradiates the atom's cloud of inertons and its neighbor completely absorbs the cloud [24].

In nuclear physics the proton and neutron are different only in their isospin projection. However, this notion does not seem fundamental but simply is useful in the appropriate algebra. Indeed,
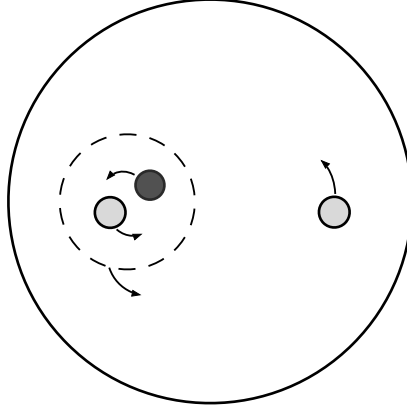
19

Figure 10: Nucleon. The pion, i.e. $\pi^0$-meson, which can be treated as an inner vortex, is rotated together with quark d (the case of the proton) or with the magnetic monopole $g_u$ (the case of the neutron). The pion and the quark d produce their own vortex in the proton. The pion and the magnetic monopole $g_u$ produce the vortex in the neutron.

what is the isospin? It is a phenomenological notion, which rather has no physical sense. It appears in some mathematical abstract considerations, that is all. For instance, for an individual *homo sapiens* we may also introduce a notion of a "pseudospin", why not? In fact: one projection of *homo sapiens* is the male, the other projection is female. Is there any benefit of such a determination?

We may suggest the structure of a nucleon as depicted in Fig. 10. Namely, instead of the generally accepted view that the structure of the proton and the neutron respectively are $p = d\,u\,u$ and $n = d\,d\,u$, we may suppose a couple of other versions for the formulas of nucleons. It seems the more plausible are $p = d\,u\,u$ and $n = d\,u\,g_u$, or in the explicit form

$$p^+ = (du,\ u) = (\pi^0,\ u), \qquad n^0 = (d\,u,\ g_u) = (\pi^0,\ g_u) \tag{53}$$

where the structure of $\pi^0$ is defined above (50).

Fig. 10 illustrates how the nature avoids the problem of three bodies, which does not have a steady-state solution: Initially two quarks form a stable vortex system; then this system jointly with one more quark/monopole forms another vortex stable system.

As is known, $W^\pm$ bosons are mediators of neutrino emission and absorption. Their charge manifests itself through emission or absorption of electron/positron. The emission of a $W^+$ or $W^-$ boson by a baryon either raises or lowers its electric charge by one unit, and also changes the spin by one unit. These bosons cause nuclear transmutation. The $Z^0$ boson is detected as a force-mediator whenever neutrinos scatter elastically from matter and their appearance is not accompanied by the production or absorption of new charged particles. Three bosons $W^\pm$, $Z^0$ and the photon represent the four gauge bosons of the electroweak interaction. Let us look how the bosons of the weak interaction appear in the submicroscopic approach.

A decay of a hadron takes place mostly under an impact of perturbative conditions. In other words, spontaneous pairs of quark-antiquark must stimulate the decay. For instance, in the framework of the submicroscopic approach the decay of the neutron (presented below as a combination of quarks d and u, and the magnetic monopole $g_u$) occurs at the collision with a quark-antiquark pair $u\bar{u}$ by the following formula:

$$(d\,u\ +\ g_u) + \{u\bar{u}\} \quad \rightarrow \quad (du\ +\ g_u + u + \bar{u}) \quad \rightarrow \quad (d\,u\ +\ u + g_u)$$

$$\rightarrow \quad (d\,u\ +\ u)\ +\ (\bar{u}\,g_u). \tag{54}$$

That is, we have obtained

$$n^0\ \rightarrow\ p^+ + W^-, \tag{55}$$

or in other words, we just revealed the inner structure of the combined particle $W^-$: $W^- = (\bar{u}\, g_u)$. This boson is composed of the antiquark $\bar{u}$ and the u-quark's magnetic monopole $g_u$, which rotate around each another (note an idea about a compositeness of $W^\pm$ and $Z^0$ bosons has already been expressed [89] in the framework of the Next-to-minimal supersymmetric standard model). Under the compressing pressure (44) this combined particle collapses in a short time of around $3 \times 10^{-25}$ s, such that each of the components changes its quark state (Fig. 3$b$) to the appropriate lepton state (Fig. 3$a$). Namely,

$$W^- \equiv (\bar{u}\, g_u) \quad \rightarrow \quad \left(e^-,\ \bar{\nu}_e\right) \quad \rightarrow \quad e^- +\ \bar{\nu}_e. \qquad (56)$$

Then the antiparticle to the boson (56) is

$$W^+ \equiv (u\, g_{\bar{u}}) \quad \rightarrow \quad \left(e^+,\ \nu_e\right) \quad \rightarrow \quad e^+ +\ \nu_e. \qquad (57)$$

The third boson of the weak force seems to have the structure

$$Z^0 = (u\bar{u}) \quad \rightarrow \quad \left\{ \begin{array}{l} \gamma\ +\ \gamma \\ \mu^+ + \mu^- \end{array} \right. . \qquad (58)$$

The moving electron is shown in Fig. 6 (right). The antineutrino can be seen in Fig. 6 (left) at the point $\lambda/2$. The antineutrino travels without changes in its monopole state along the whole path. Because at the creation of a pair of particle-antiparticle, the particle and the antiparticle emerge only in the electric state; the magnetic monopole state is an interjacent state (Fig. 6) and without the accompanying inerton-photon cloud this state cannot be changed (about the motion of a charged particle see Ref. 26 for details).

Fig. 11 depicts a typical structure of a hadron that consists of a quark q and antiquark $\bar{q}$; such a pattern is typical for $\pi^0$-mesons, $Z^0$-bosons and similar hadrons.

Fig. 12 pictures a typical structure of a hadron that consists of a quark q and the magnetic monopole $g_{\bar{q}}$; such a pattern is typical for $\pi^\pm$-mesons, $W^\pm$-bosons and similar hadrons.

At a fast non-adiabatic process (annihilation, explosion, decay) the magnetic monopole can be released from the combined hadron in question breaking the sound barrier in the tessellattice, which is the velocity of light $c$. Coming through the barrier the quark state collapses to the lepton state (the transition from Fig. 3$b$ to Fig. 3$a$) and the quark's magnetic monopole becomes the corresponding lepton's magnetic monopole. This lepton's monopole is known as a neutrino that travels with the velocity close to $c$. In its motion the neutrino interacts with cells of the tessellattice and generates a cloud of inertons. The motion should obey relationships (27). With a neutrino energy around 1 GeV (i.e. $mc^2 = 1$ GeV $= 1.6 \times 10^{-10}$ J) we may estimate its velocity $v_{\text{neutrino}}$ equal to about $c$ (maybe $0.99c$). We deduce from relationships (27) the neutrino's de Broglie wavelength $\lambda \sim 10^{-16}$ m and the frequency $\nu \sim 10^{24}$ Hz of the neutrino oscillations along its path. In transversal directions the neutrino's inertons reach a distance $\Lambda = \lambda\, c/v_{\text{neutrino}} \approx \lambda \sim 10^{-16}$ m. The larger the neutrino's energy, the shorter is $\lambda$ and the smaller $\Lambda$, though the frequency $\nu$ grows. In each odd section $\lambda/2$ of the neutrino's path it emits inertons and gradually loses its velocity and mass; during each even section $\lambda/2$ the neutrino re-absorbs its inertons and restores its mass, and inertons colliding with the neutrino reset its initial velocity, and so on.

If the neutrino starts to move with the speed $v_{\text{neutrino}} > c$, then at impacts with oncoming cells of the tessellattice the neutrino will excite them, so that after passing a cell, the cell will quickly relax, generating an inerton and/or photon in transversal directions. And such motion signifies a kind of a real friction (the bremsstrahlung). Tracks of $\gamma$-quanta after passing of a neutrino have never been observed; this means that the speed of neutrinos is less than $c$ (see also Ref. 90).

## 4.3. On the structure of a nucleon

Nuclei are bound together by the residual strong force (the nuclear force), as QCD claims. On the other hand, because of the well-known difficulty of QCD in the non-perturbative domain, many effective models reflecting the characteristics of the strong interaction are used to study the behavior of nucleons. QCD remains indispensable in the study of nuclear phenomena of the quark
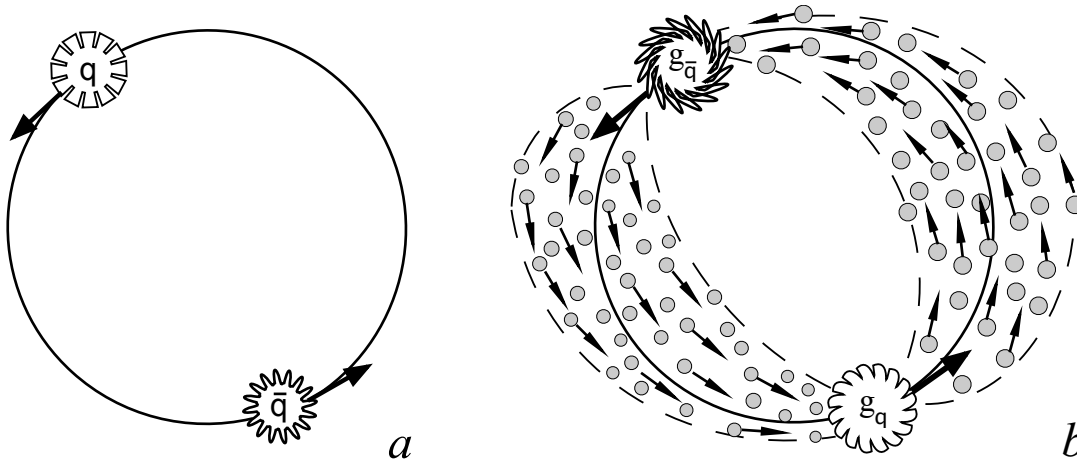
Figure 11: Hadron formed by the quark q (with the charge $-e$) and the antiquark $\bar{\text{q}}$ (with the charge $+e$). $a$ – the quark q and the antiquark $\bar{\text{q}}$ are found in the initial state; $b$ – each of the quark q and the antiquark $\bar{\text{q}}$ has passed the section $\lambda/2$ of their paths and their state is transformed: q $\rightarrow$ g$_q$ (i.e. from the quark state to the monopole state) and $\bar{\text{q}} \rightarrow$ g$_{\bar{\text{q}}}$ (i.e. from the antiquark state to the antimonopole state). Then passing the next section $\lambda/2$ these entities interacting through spatial inflated excitations, i.e. qinertons, change the configuration to the initial state (Figure $a$): the quark q and the antiquark $\bar{\text{q}}$, respectively. And so on.

structure of the nucleon. To such models belongs the MIT bag model, the Friedberg-Lee soliton bag model [91], the quark-meson coupling model [92, 93], the $\pi - \rho - \omega$-meson coupling Skyrme soliton model [94] including an effective nucleon-nucleon force of the Skyrme type [92], the chiral $SU(3)$ quark model [96, 97], the quark mass density-dependent model and the quark mass density- and temperature- dependent model [98], the chiral soliton model where baryons are described as non-topological solitons [99], and others.

The meson theory of nucleon coupling, i.e. a pion exchange between nucleons, does not look as a logical mechanism that binds the nucleons: the energy of pions is around 140 MeV, which is only 6.7 times less than the energy of the nucleon. How often are these pions emitted by one nucleon and absorbed by another? What is the duty cycle? What is the mechanism of the emission? Comay [100] showed that the Yukawa theory proposed in the past to describe the nuclear forces is undergoing significant theoretical difficulties and inconsistency; an analogous argument proves that a Yukawa particle cannot be associated with the real $\pi^0$-meson.

High precision measurements [101] of the deuteron electromagnetic structure functions ($A$, $B$ and $T_{20}$) extracted from high-energy elastic $ed$ scattering, and the cross sections and asymmetries extracted from high-energy photodisintegration $\gamma + d \rightarrow d + n$ allowed the authors to conclude that the experiments do not prefer any of the approaches: the residual quark-gluon interaction and the meson exchange. Moreover, both approaches seem to disagree. The authors tested theoretical considerations that included non-relativistic and relativistic models using the traditional meson and baryon degrees of freedom, effective field theories, and models based on the underlying quark and gluon degrees of freedom of QCD, including non-perturbative quark cluster models and perturbative QCD.

Among new approaches to the problem of the origin of nuclear forces we can mention Santilli's [102] approach based on the introduction of hadronic mechanics, which operates with a nonunitary transform of orthodox quantum mechanics, i.e. in the approach, which is algebraic, due to the strong interaction, one cannot separate the kinetic and potential energy in the nuclear system
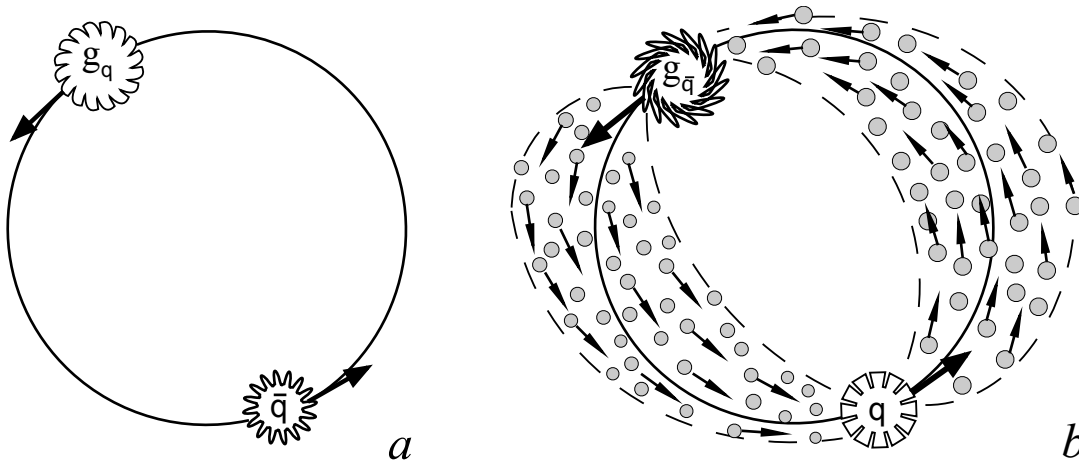
Figure 12: Hadron formed by the magnetic monopole $g_q$ of the quark q (with the charge $-e$) and the antiquark $\bar{q}$ (with the charge $+e$). $a$ – the magnetic monopole $g_q$ and the antiquark $\bar{q}$ are found in the initial state; $b$ – each of the entities, the monopole $g_q$ and the antiquark $\bar{q}$, has passed the section $\lambda/2$ of their paths and their state is transformed: $g_q \rightarrow q$ (i.e. from the monopole state to the quark state) and $\bar{q} \rightarrow g_{\bar{q}}$ (i.e. from the antiquark state to the antimonopole state). Then passing the next section $\lambda/2$ these entities interact through spatial inflated excitations, i.e. qinertons, and change their configuration to the initial state (Figure $a$): the magnetic monopole $g_q$ and the antiquark $\bar{q}$, respectively. And so on.

studied.

The author [27] carried out a preliminary study of the problem of nuclear forces in the framework of the submicroscopic approach a few years ago. Taking into account the study [27] we may now consider a nucleus in more detail.

Let us initially unify quarks d and u to the $\pi^0$-meson state (50), as is shown in Fig. 10. For this we shall solve the problem of two bounded charged particles (see, e.g. Ref. 103), which in our case of two quarks in addition they are bounded through the potential of the strong force. For the Coulomb interaction of the quarks d and u the potential is

$$V_{\text{Coulomb}} = -\frac{e^2}{4\pi\varepsilon_0 |r_{\text{d}} - r_{\text{u}}|} \qquad (59)$$

where $r_{\text{d}}$ and $r_{\text{u}}$ are coordinates of the quarks. For the strong interaction of the quarks d and u (in the interior of the bubble, Fig. 9), which occurs through qinertons, the potential is

$$V_{\text{strong}} = -\frac{h\,c}{|r_{\text{d}} - r_{\text{u}}|}. \qquad (60)$$

Since the ratio $V_{\text{strong}}/V_{\text{Coulomb}} \cong 137.1597 \times 2\pi$, we may neglect the potential (59). The potential (60) is completely non-perturbed and deals with energies less than 10 MeV, therefore, such presentation (60) does not contradict with data analyzed by Bethke [33]. Then the Lagrangian that describes two bounded quarks reads

$$L = \tfrac{1}{2}m_{\text{d}}\dot{r}_{\text{d}}^2 \, + \, \tfrac{1}{2}m_{\text{u}}\dot{r}_{\text{u}}^2 \, - \, \frac{h\,c}{|r_{\text{d}} - r_{\text{u}}|}. \qquad (61)$$

We can pass on to the coordinate of the center of gravity $r_{\text{c.g.}} = (m_{\text{d}}r_{\text{d}} + m_{\text{u}}r_{\text{u}})/(m_{\text{d}} + m_{\text{u}})$ and the relative coordinate $r = r_{\text{d}} - r_{\text{u}}$, which then changes the Lagrangian (61)

$$L = \tfrac{1}{2}(m_{\text{d}} + m_{\text{u}})\,\dot{r}_{\text{c.g.}}^2 \, + \tfrac{1}{2}\mu\,\dot{r}^2 - \frac{h\,c}{r} \qquad (62)$$

where the reduced mass is

$$\mu = m_{\text{d}}\,m_{\text{u}}/(m_{\text{d}} + m_{\text{u}}). \qquad (63)$$

Let the centre of gravity be motionless; then the first term in Lagrangian (62) becomes zero.

Now we can solve the Schrödinger equation (36) having preserved the two last terms in the Lagrangian (62) in which we can insert the relativistic masses of the quarks. The result is the problem of the hydrogen atom whose solution is known. In particular, we can write the radius of the orbit for the reduced mass $\mu$. In the conventional case of the hydrogen atom, this is the Bohr radius

$$r_{\text{Bohr}} = \frac{\hbar^2}{m_{\text{electron}}\frac{e^2}{4\pi\,\varepsilon_0}}. \qquad (64)$$

For the case of the strong potential (60) the solution for the radius of the reduced mass $\mu$ is

$$r_0 = \frac{\hbar}{2\,\pi\,\mu\,c}. \qquad (65)$$

Let us first consider a free $\pi^0$-meson. Its energy is 135 MeV. We may put for the u and d quarks the rest energy 3 and 5 MeV, respectively; then their total energies in the $\pi^0$-meson respectively are 50.625 MeV and 84.375 MeV. From expression (63) we get for the reduced meson mass $\mu_{\pi^0} = 5.6325 \times 10^{-29}$ kg. Substituting this value into the expression (65), we obtain $r_{0,\,\pi^0} = 0.99 \times 10^{-15}$ m.

Now we can consider a nucleon. In the proton an energetic $\pi^0$-meson and a quark u rotate around one another; in the neutron $\pi^0$-meson and the u-quark's monopole $g_{\text{u}}$ are rotating around each other. We shall emphasize that since two particles are found in the same orbit, the section between them along the orbital path is equal to the de Broglie wavelength for each of the particles.

How is the energy $E_{\mathrm{nucleon}} = 939$ MeV distributed among the $\pi^0$-meson and its rotating partner? Let $3/4 \cdot E_{\mathrm{nucleon}}$ accounts for the $\pi^0$-meson (because it consists of two particles and as the whole the meson is also a particle) and $1/4 \cdot E_{\mathrm{nucleon}}$ for its partner (the quark u for the proton or the monopole $g_u$ for the neutron). In such case the mass of the reduced particle in the nucleon is $\mu_{\mathrm{nucl}} = m_{\pi^0}\, m_{\mathrm{u}}/(m_{\pi^0} + m_{\mathrm{u}}) \cong m_{\pi^0}\, m_{g_{\mathrm{u}}}/(m_{\pi^0} + m_{g_{\mathrm{u}}}) \cong 3.71 \times 10^{-28}$ kg. After that we can calculate the radius of the orbit of this reduced particle by using expression (65):

$$r_{0,\,\mathrm{nucl}} = 0.2 \times 10^{-15}\mathrm{m}. \tag{66}$$

The cloud of qinertons for the reduced mass $\mu_{\mathrm{nucl}}$ has amplitude

$$\Lambda \approx \lambda_{\mathrm{de\,Brog}}\, c/v + r_{0,\,\mathrm{nucl}}\big|_{v \cong c} = \pi r_{0,\,\mathrm{nucl}} + r_{0,\,\mathrm{nucl}} \approx 0.83 \times 10^{-15} \text{ m}, \tag{67}$$

which does not exceed the radius of the unified bubble created around the nucleon's three quarks, i.e. the amplitude of the cloud of qinertons is less than the Compton wavelength of the nucleon: $\Lambda < \lambda_{\mathrm{Com,\,nucl}} = 1.32 \times 10^{-15}$ m. Therefore, qinertons generated of the quarks in motion are located strictly inside of the nucleon, namely, in the range limited by the radius $\Lambda \approx 0.83 \times 10^{-15}$ m.

Now we can turn to recent experimental data [104]: The physical picture is that the proton is comprised of three regions: an outer cloud of q$\bar{\mathrm{q}}$ condensed ground state of size $r_{\mathrm{q\bar{q}}} \geq 0.86 \times 10^{-15}$ m, an intermediate shell of baryonic charge of size $r_{\mathrm{B}} = 0.44 \times 10^{-15}$ m, and a core of size $r_{\mathrm{c}} = 0.2 \times 10^{-15}$ m, where valence quarks are confined.

The same authors [105, 106] further note that these experimental results allow a description in terms of the topological soliton model of the nucleon. For this purpose they introduce an abstract scalar field $\varsigma$ of an undetermined nature. Manipulating with the $\varsigma$ they arrive at the topological soliton model in which the large mass problem is resolved by tearing the scalar field $\varsigma$ at the critical size $r_{\mathrm{c}} = 0.2 \times 10^{-15}$ m, i.e. the pion decay coupling constant $f_{\pi}$ $(= 93$ MeV) [106], drops down sharply to zero at $r < r_{\mathrm{c}}$, which decreases the mass of the soliton by a significant amount; this allows them to associate the model with a chiral bag model. The region $r_{\mathrm{c}} < r < r_{\mathrm{B}}$ was called the shell of topological baryonic charge density. At $r > r_{\mathrm{B}}$, the scalar field $\varsigma$ decreases smoothly, which makes here the quarks and antiquarks massive and lowers the energy of the Dirac sea. Hence, the region $r_{\mathrm{B}} < r < r_{\mathrm{q\bar{q}}}$ should represent a q$\bar{\mathrm{q}}$ condensed ground state that forms an outer cloud of the proton.

Such a topological soliton model of the proton was called a 'Condensate Enclosed Chiral Bag' [106]. In the end the authors assert: "The consequent discovery of the structure of the proton at LHC at the beginning of the 21st century will be analogous to the discovery of the structure of the atom from high energy $\alpha$-particle scattering by gold atoms at the beginning of the 20th century." A similar Skyrme model in which chiral rotation of the scalar and pseudo-scalar fields lead to the linear sigma model favoring the identification of the scalar field to the scalar sigma was developed in work [107].

Nevertheless, from the physical point of view, a non-topological soliton model [90] looks more preferable. Indeed, a bag model exhibits physical characteristics very similar to those of a "gas bubble" immersed in a "medium": the model operates with a constant surface tension and a constant pressure exerted by the medium on the gas in the bubble; besides, the model includes the thermodynamic energy of the gas and the related gas pressure.

The submicroscopic description of the behavior of quarks presented above agrees rather with the physical pattern of a "gas bubble" constructed in Ref. 91. Let us now compare our theoretical results with the experimental data [106]:

1) a core of size $r_{\mathrm{c}} = 0.2 \times 10^{-15}$ m, where valence quarks are confined – this exactly corresponds to the radius (66) of the orbit of the reduced particle of the nucleon;

2) an outer cloud of q$\bar{\mathrm{q}}$ condensed ground state of size $r_{\mathrm{q\bar{q}}} \geq 0.86 \times 10^{-15}$ m – this conforms to the amplitude (67) of the cloud of inflated excitations generated by the reduced particle in the nucleon;

3) an intermediate shell of baryonic charge of size $r_{\mathrm{B}} = 0.44 \times 10^{-15}$ m – this is the inflection point of the static quark potential (6), which in the explicit form combining

25

expressions (43) and (60) can be read

$$V(r) = -\sigma r - hc/r. \tag{68}$$

In this potential the two terms are negative and they describe attraction. The first term is negative, because it is stipulated by the mechanism of the attraction of bubbles, expressions (42) and (43). The second term is dictated by a spherical standing wave generated by each of the quarks in the system under consideration: the quark periodically decomposes, i.e. it throws off its inflated state by portions and the standing spherical wave spreads these qinertons along a relief given by the deformation coat of the quark (Fig. 3$b$); it is this peculiar relief that directs two quarks – through their qinertons – to each other. The extremum of the Eq. (68) is reached at the solution of the equation $dV/dr = 0$, i.e. $\sigma - hc/r^2 = 0$. This equation gives the solution for the inflection point

$$r_{\text{inf}} \cong \sqrt{hc/\sigma} \tag{69}$$

that can be identified with the shell of baryonic charge $r_{\text{B}} = 0.44 \times 10^{-15}$ m of Ref. 104. In the point $r = r_{\text{inf}}$ the potential (68) is maximal, as $V''(r_{\text{inf}}) < 0$, which means that at $r = r_{\text{inf}}$ the attraction is minimal.

Thus Nature does not solve the problem of three bodies; Nature reduces the problem to a system of two bodies, which allows an analytical solution, as has been discussed above.

Expression (69) allows us to estimate the value of the surface tension of the quark's bubble. Indeed, for the constant $\sigma$ we get $\sigma = hc/r_{\text{inf}}^2 \cong 1.027 \times 10^6$ Jm$^{-1}$. With account for expressions (42) and (43), we obtain an estimate of the tension of the quark's bubble:

$$\gamma = \sigma/(4\pi\chi) \sim 10^{20} \text{ Nm}^{-1} \tag{70}$$

where we set the depth of overlapping $\chi \sim 10^{-16}$ to $10^{-15}$ m (see Fig. 8). For example, for some liquid substances typical values of the surface tension at a room temperature are: 0.465 Nm$^{-1}$(mercury), 0.073 Nm$^{-1}$ (water) and 0.03 Nm$^{-1}$ (soap water).

According to the theory described above a nucleon is a typical bubble and its surface film (interface, or membrane) is specified by the thickness from $r = \Lambda \approx 0.83 \times 10^{-15}$ m to $r = \lambda_{\text{Com, nucl}} = 1.32 \times 10^{-15}$ m. Such a bubble with the membrane is shown in Fig. 13.

It is interesting that proton charge radii obtained from electronic measurements and the hydrogen spectroscopy settle around 0.88 fm, whereas the proton radius obtained from muonic hydrogen experiments is at 0.84±0.01 fm [108-110] and the researchers noted the real size is rather 0.84±0.01 fm, which is exactly the case (67) derived from the inner consideration of the constitution of a nucleon described in the present work.

Beta decay of the neutron, which outside a nucleus has a lifetime of about 15 minutes, is denoted by the radioactive decay

$$n^0 \to p^+ + e^- + \bar{\nu}_e.$$
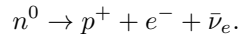
Where do the electron and the electron antineutrino come from? Nobody knows. Nevertheless, expressions (54)-(56) clarify the process of transformation in the real space constituted as the tessellattice. Figure 14 depicts vividly successive changes in the process of neutron transformation: ($a$) the initial stable state of the neutron; ($b$) the separate orbital monopole $g_{\text{u}}$, which is the axial state of the quark u$^+$, scatters by the oncoming virtual quark-antiquark pair (u$^+$, ū$^-$). Such pairs can be created from the tessellattice only in the electrically charged state and never in the monopole state; ($c$) the quark u$^+$ substitutes for the monopole $g_{\text{u}}$ occupying the orbit of the latter and at the same time the antiquark ū$^-$ and the monopole $g_{\text{u}}$ leave the nucleon as an unstable pair of ū$^-$ and $g_{\text{u}}$ known as a virtual particle $W^-$. The separating particles ū$^-$ and $g_{\text{u}}$ cannot exist in the tessellattice in the inflated state. That is why the tessellattice immediately squeezes ū$^-$ and $g_{\text{u}}$ to the state of local stable deformations and they become the electron $e^-$ and antineutrino $\bar{\nu}_e$, respectfully. In this phase transition from one topology to the other, only the particles' volumes change (from Fig. 3$b$ to Fig. 3$a$); their surface polarizations are preserved.
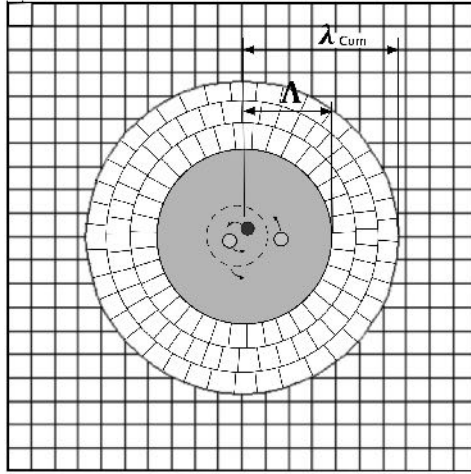
Figure 13: Structure of a nucleon. The quarks are rotated in the interior of the nucleon, which is shown as the grey sphere having the radius $r = \Lambda \approx (0.83 - 0.86) \times 10^{-15}$ m. The membrane of the bubble spreads from $r = \Lambda$ to $r = \lambda_{\mathrm{Com,\,nucl}} = h/(m_{\mathrm{p\,(n)}}c) = 1.32 \times 10^{-15}$ m. In the membrane cells of the tessellattice are found in a stretched state and the cohesive forces between these cells are responsible for the surface tension.
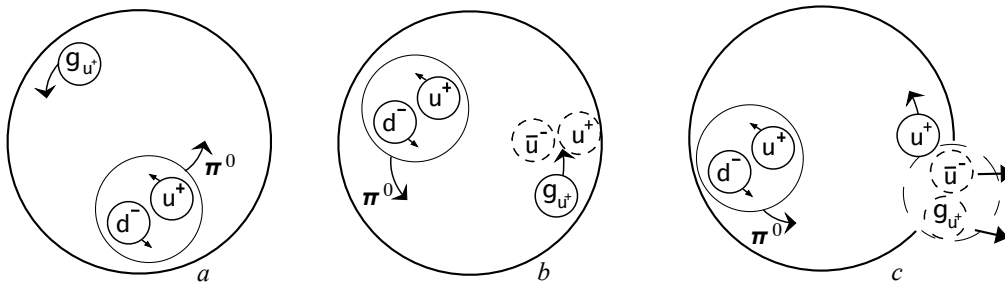


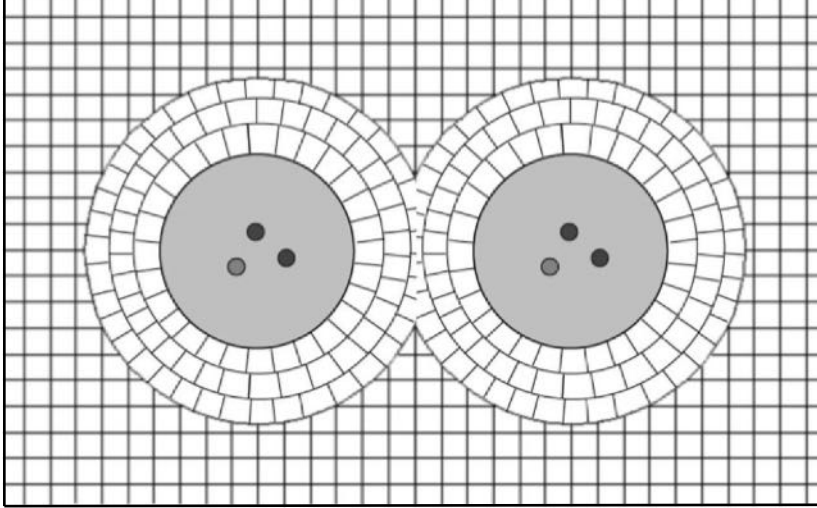Figure 14: Beta decay of the neutron to the stable state of the proton.

Figure 15: Attraction of two nucleons is cause by the adhesion of their membrane films.

The present study unveils the inner nature of the nuclear forces: the attraction between motionless nucleons is caused by their adhesion. Two membranes stick together generating a stable formation shown in Fig. 15. Note in nuclear physics the radius of nuclear forces reaches $(1.2 - 1.5) \times 10^{-15}$ m [111], which is compatible with our result $\lambda_{\text{Com, nucl}} = 1.32 \times 10^{-15}$ m. At a distance around 0.4 fm the nuclear forces of attraction are changed to forces of repulsion [112], which is also consistent with our result, as this is the inflection point (69) of the quark potential (68). In motion a nucleon generates its own inerton cloud that accompanies the nucleon, as Fig. 4 exhibits. Since in nuclei the speed of a nucleon is less than the velocity of light and the energy per nucleon is about 8 MeV, we may estimate the average nucleon's de Broglie wavelength as about $\lambda \approx 5 \times 10^{-15}$ m and the nucleon's inerton cloud, which spreads around the nucleon (see Fig. 4), reaches the distance of around $\Lambda = \lambda c/\upsilon \sim 10^{-14}$ m. An inerton theory of the interaction of nucleons was developed in Ref. 27. Of course perturbations should generate virtual pairs of lepton-antilepton and/or quark-antiquarks in the vicinity of the quantum system studied. These pairs have to disturb the Lagrangian of nucleon–nucleon interaction presented in Ref. 27.

The problem of the proton spin crisis has been discussed in the literature for years (see, e.g. recent experimental works [113-115]). The quarks inside a proton have their own intrinsic spin. But numerous experiments have confirmed that a directional preference among all these quark spins can account for only about 25% of the proton's total spin. Therefore, gluons contribute much less than originally speculated to proton spin, so the source of the spin still remains a mystery.

Camay [116] notes that the problem would be solved if one correctly calculates angular momentums of all the quarks and takes into account the quark spatial motion (which also is in agreement with experiment [113]). Nevertheless, to resolve the problem of the proton spin, one first has to have a correct determination of the notion of spin as such. The determination was done in works [23, 22]: spin-1/2 is an integral property of a moving particle, which is associated with a kind of inner pulsations/oscillations. These oscillations may have two opposite directions, which set two opposite projections. The projections of oscillations may be related to the direction of the particle's electro-magnetic polarization, left or right. The electro-magnetic polarization is given by the needles on the surface of the particle, which is described by the Maxwell equations [22]. Hence any charged particle moves like an oscillating vortex with the left or right surface polarization (i.e. left of right polarized electro-magnetic filed). The inerton cloud of a charged particle being electromagnetically polarized carries the phenomenon of the particle's spin (the left or right oscillating electromagnetic vortex) through the space.

In the case of the proton, probing the structure of the proton for its spin, one has to use low

energy collisions and prolong the duration of the reaction until the proton passes its whole de Broglie wavelength $\lambda \approx 5 \times 10^{-15}$ m.

At a higher energy (a few to hundreds of GeV) the length of its de Broglie wavelength $\lambda$ falls within its size, i.e. $\lambda$ becomes less than $\lambda_{\mathrm{Com, \ p}}$. In this case the experiment will probe the motion of the proton's entities – quarks – and the data will be specified by dispersion (a similar situation takes place in femtosecond optics: a probing laser pulse fixes a "frozen" instantaneous state of complete vibrations of atoms).

# 5. Discussion and conclusion

We have reviewed the mainstream concepts aimed at the description of elementary particles in the high-energy domain. The majority of existing approaches are developing in the realm of abstract phase spaces, which introduces significant difficulties in physical interpretation of their notions. For example, color charges of quarks, which supposedly have to compensate each other at the interaction, cannot be measured in principle. Even in the framework of QCD the concept of the integer quark charge is working very well [52, 54], so no sense to introduce any fractional charges that are not observed experimentally. Many discrepancies of QCD were considered by Comay [116-118]; in particular, he [117] emphasizes that QCD has no theoretical explanation for the interaction of a hard photon with hadrons; an old idea of vector meson dominance suggested to explain the interaction properties of high-energy photons with hadrons is strongly criticized.

All events of high-energy physics occur in the background of an ordinary physical space, though the major modern quantum concepts refer to this background as to a vague vacuum with unknown and undetermined properties. An ambiguous physical vacuum really introduces a concept of god and devil in modern science. In fact, the vacuum brings particles to existence from its dark body and takes the particles back. As a result we already got dark matter and dark energy. Of course such pseudo physical doctrine of the physical vacuum requires a redefining.

The physical vacuum was reconsidered in our works [16-19] in terms of a physical space. The structure of physical space was derived from first mathematical principles by using topology, set theory and fractal geometry. The examination immediately sheds light on the scene of all the events of elementary particles. The theory explains what is a real particle (lepton and quark), what are its size and shape, what is its mass, what are its properties, how it interacts with the space that just created it, and how the particle moves satisfying all the peculiarities of quantum mechanics [20-28]. Those studies allow us to apply the developed submicroscopic concept to the physics of quarks, which has been done in the present work.

It has been argued that the quark represents an inflated cell in the tessellattice and around this kernel-cell a coat is developed to compensate the inflation. Beyond the deformation coat the space remains unperturbed. The interaction of quarks occurs through an agglutination of their coats, which are typical bubbles filled with inflated excitations produced by standing spherical waves generated by the quarks. A short-range interaction of bubbles easily resolves the paradox of confinement and asymptotically freedom of quarks. We have analyzed the stability of such physical picture, in particular, for the proton. The conclusion has been drawn that unperturbed nucleons interact through two major channels: i) a direct coalescence of the nucleons? deformation coats and ii) the spatial excitations generated by the nucleons at the motion through space [27]. These excitations are *inertons*, which were introduced in previous papers by the author [20-28]. The concept of inertons was proven in a number of different experiments (see, i.e. Refs. 28, 119).

From the viewpoint of the structure of the tessellattice, there are no reasons to introduce fractional charges for quarks. The structure of quarks and hadrons presented in section 4 introduces the integer charge for quarks $\pm e$. The present theory focuses on a dynamic pattern: how quarks move, what are their trajectories inside of a hadron, at which configurations the quarks enter the hadron under consideration (i.e. the electric state or the magnetic monopole state), etc. The quark's cloud of inflated excitations named *qinertons* allows a direct connection to a gluon of QCD. In the approach developed the quark is colorless. No sense to introduce an additional kind of the interaction caused by some "colors", because quarks with their qinerton clouds represent

29

Figure 16: Laboratory apparatus of the Lx series produced by the company Indra Scientific SA, which generates inerton fields.

real bubbles in the tessellattice and these bubbles interact with a potential proportional to $r$, as described above in the present work, which binds quarks.

The isospin phenomenology can be substituted by deterministic submicroscopic dynamics of bubbles with the quarks in the bubble's center. Such dynamics, a kind of a hydrodynamics with elements of submicroscopic mechanics is not developed yet. A new mathematics will be needed for the description and understanding of these systems: tightly interacting bubbles in which kernel particles (quarks, or partons) with qinertons (whose cloud is a gluon?) are dancing under their own mechanics. Such studies will be able to shed light on the criterions of stability/non-stability of hadrons.

The theory can further be tested in scattering experiments, as it allows the calculation of form factors and the differential cross-section for elastic scatterings of the hadrons studied.

In our recent studies we revealed that inerton fields produced at rather simple laboratory conditions are able to influence not only chemical, physical and biological processes, but also nuclear reactions. An apparatus that generates inerton fields is illustrated in Fig. 16. Below we state two examples of using the inerton field.

Figure 17 shows spectra of a sample of radioactively contaminated water, 300 ml, whose initial radioactivity was about $10^{-5}$ Bq/l. After 30-second processing of the water sample with the inerton field having the intensity of a few thousand pulses per second, the level of radioactivity was quenched by 32%. Further treatment did not reduce the level of radioactivity of water – we reached a saturation threshold. It seems a further quenching could be possible at a heightening of the intensity of applied inerton field.

Cylindrical samples with the length 15 mm and the diameter 1 mm made of technical iron were affected by inerton fields in the apparatus Lx (Fig. 15) for 30 seconds. The structure of the control sample, which was studied with the use of a JEOL electron microscope, is shown in Table 1 and Fig. 18. The elemental composition of the sample affected by inerton fields is shown in Table 2,$a$, $b$, and $c$ and Fig. 18, 19, 20, respectively (the elemental composition was analyzed in three different points $a$, $b$ and $c$ of the sample).
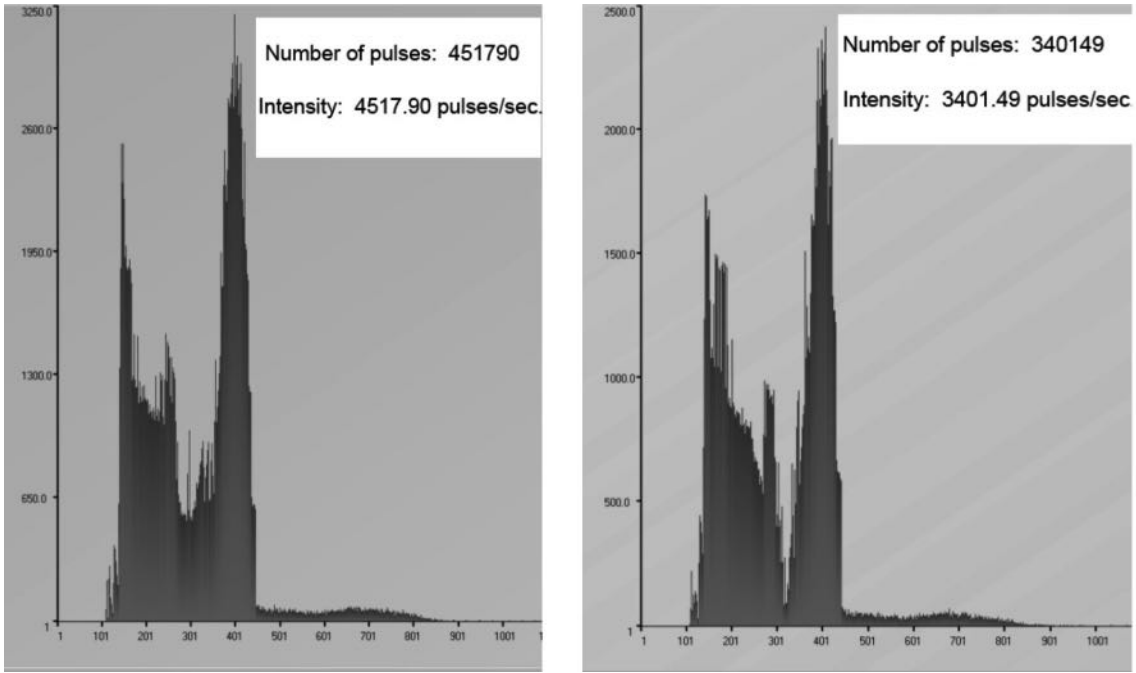
Figure 17: $\gamma$-spectra of a sample of radioactive water before processing of inerton field (left) and after processing (right). The numbers of pulses of $\gamma$-quanta recorded by the scintillator are shown in the upper right corners of the graphs.
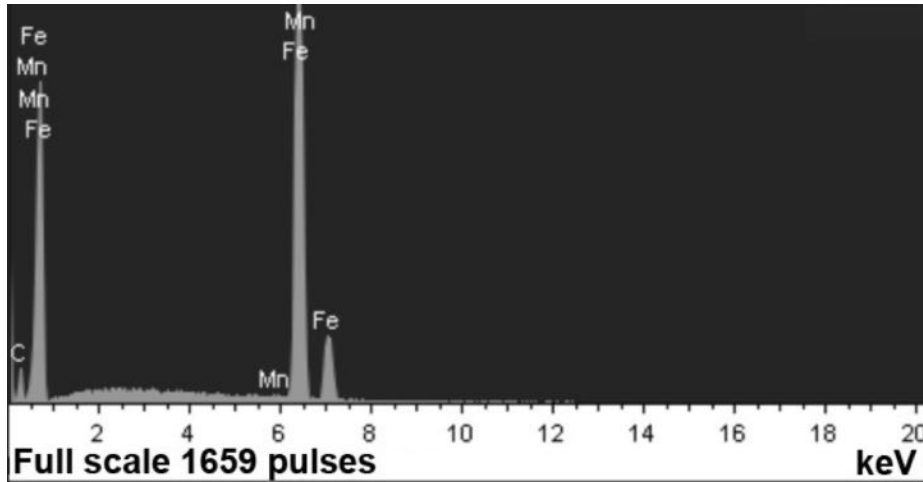


Figure 18: Elemental composition of the iron sample (control).

**Table 1** (See Fig. 18.)

| Element | Composition, % | Atomic, % |
|---------|----------------|-----------|
| C K     | 11.72          | 8.16      |
| Mn K    | 0.39           | 0.28      |
| Fe K    | 87.89          | 61.56     |
| Total    100.00 % ||  |

**Table 2a** (See Fig. 19.)

| Element | Weight, % | Atomic, % | Composition, % | Formula |
|---------|-----------|-----------|----------------|---------|
| C K     | 2.09      | 5.61      | 7.64           | $CO_2$  |
| Ca K    | 0.34      | 0.27      | 0.48           | CaO     |
| Cr K    | 0.35      | 0.22      | 0.51           | $Cr_2O_3$ |
| Mn K    | 0.38      | 0.23      | 0.50           | MnO     |
| Fe K    | 68.63     | 39.70     | 88.30          | FeO     |
| Co K    | 0.56      | 0.30      | 0.71           | CoO     |
| Ni K    | 1.47      | 0.81      | 1.87           | NiO     |
| O       | 26.18     | 52.86     |                |         |
| Total    100.00 % ||||  |

**Table 2b** (See Fig. 20.)

| Element | Weight, % | Atomic, % | Composition, % | Formula |
|---------|-----------|-----------|----------------|---------|
| C K | 3.57 | 9.04 | 13.09 | $CO_2$ |
| Ca K | 0.58 | 0.44 | 0.81 | $CaO$ |
| Cr K | 0.40 | 0.24 | 0.59 | $Cr_2O_3$ |
| Fe K | 63.04 | 34.31 | 81.10 | $FeO$ |
| Ni K | 1.93 | 1.00 | 2.46 | $NiO$ |
| Cs L | 0.36 | 0.08 | 0.38 | $Cs_2O$ |
| Hf L | 1.33 | 0.23 | 1.57 | $HfO_2$ |
| O | 28.78 | 54.67 | | |
| Total    100.00 % | | | | |


**Table 2c** (See Fig. 21.)

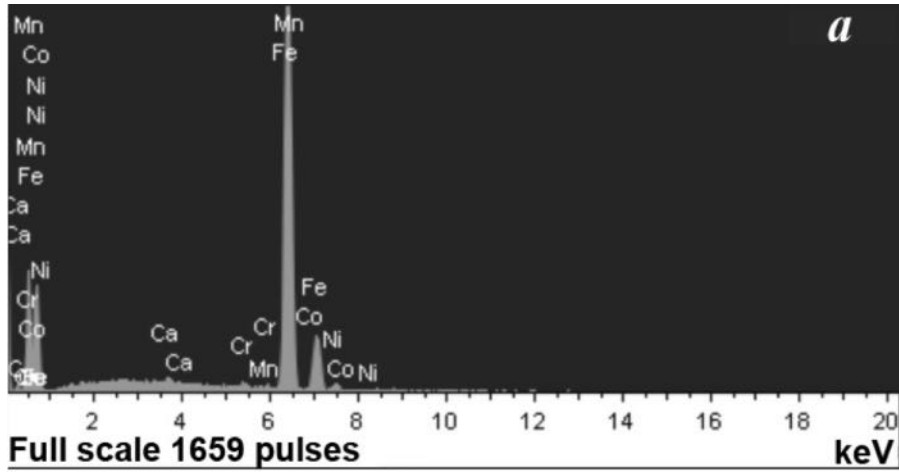| Element | Weight, % | Atomic, % | Composition, % | Formula |
|---------|-----------|-----------|----------------|---------|
| C K | 3.88 | 9.61 | 14.21 | $CO_2$ |
| Ca K | 0.48 | 0.36 | 0.67 | $CaO$ |
| Cr K | 0.34 | 0.20 | 0.50 | $Cr_2O_3$ |
| Mn K | 0.20 | 0.11 | 0.26 | $MnO$ |
| Fe K | 63.16 | 33.64 | 81.25 | $FeO$ |
| Ni K | 2.44 | 1.24 | 3.10 | $NiO$ |
| Cs L | 0.00 | 0.00 | 0.00 | $Cs_2O$ |
| O | 29.50 | 54.85 | | |
| Total    100.00 % | | | | |

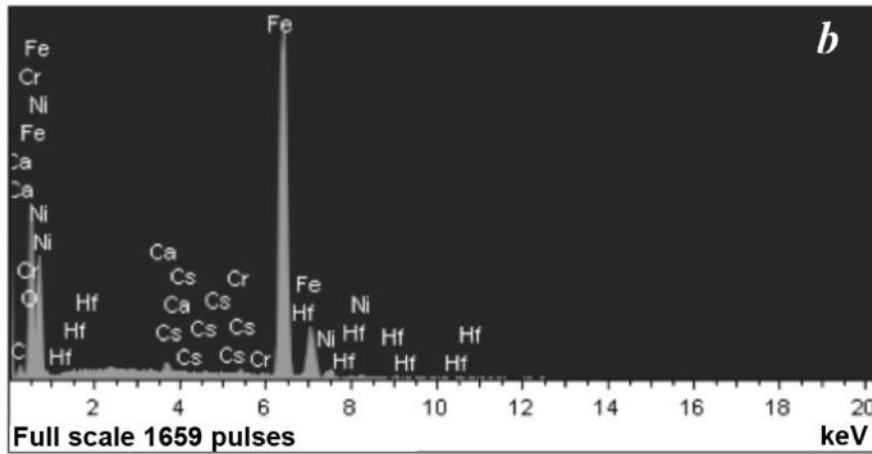Figure 19: Elemental composition in the point $a$ of the affected sample.



Figure 20: Elemental composition in the point $b$ of the affected sample.

Literature on low energy nuclear reactions is abundant [120,121], though there is no theoretical understanding of the phenomena. There are no solid theoretical ideas regarding methods of control of nuclear reactions. The study presented in this paper opens a gateway to a real realization of controlled fission and fusion reactions in which an inerton field is able to play the role of a moderator between microscopic and subatomic processes.
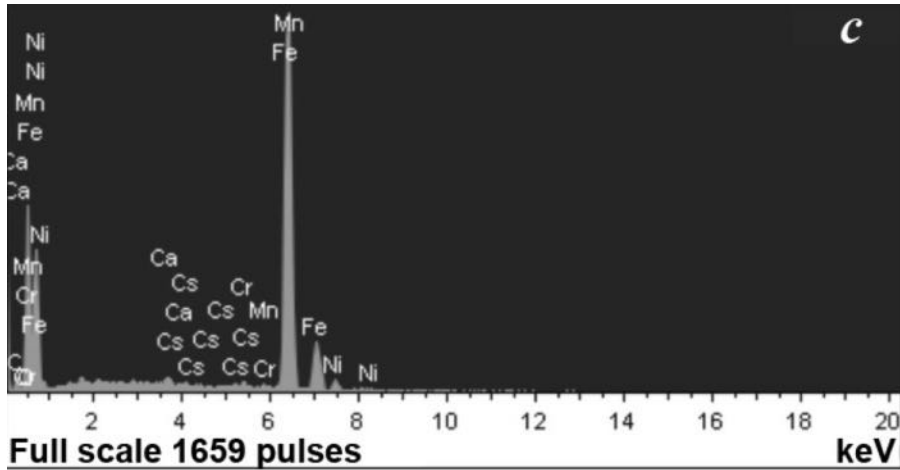
# Acknowledgment

Figure 21: Elemental composition in the point $c$ of the affected sample.

# References

1. R. Oerter, *The theory of almost everything: The standard model, the unsung triumph of modern physics* (Plume, New York, 2006).

2. F. Wilczeck, QCD made simple, *Physics Today*, **53**, no. 8, 22-28 (2000).

3. R. P. Feynman, The behavior of hadron collisions at extreme energies, in *High energy collisions: Third international conference at Stony Brook, New York*, (Gordon & Breach, 1969), pp. 237–249.

4. W. Greiner, S. Schramm and E. Stein, *Quantum chromodynamics*, 3rd. rev. and enlarged ed., Springer-Verlag, Berlin, Heidelberg, New York (2007).

5. G. Sterman, J. Smith, J. C. Collins, J. Whitmore, R. Brock, J. Huston, J. Pumplin,W.-K. Tung, H. Weerts, C.-P. Yuan, S. Kuhlmann, S. Mishra, J. G. Morfn, F. Olness, J. Owens, J. Qui, and D. E. Soper, Handbook of perturbative QCD, *Rev. Modern Phys.* **67**, no. 1, 157-248 (1995).

6. M. Jacob, *The quark structure of matter*, World Scientific Publishing Co., Singapore (2000).

7. Y. Nambu and G. Jona-Lasinio, Dynamical model of elementary particles based on an analogy with superconductivity. I, *Phys. Rev.* **122**, no. 1, 345–358 (1961).

8. Y. Nambu and G. Jona-Lasinio, Dynamical model of elementary particles based on an analogy with superconductivity. II, *Phys.Rev.* **124**, no. 1, 246-254 (1961).

9. T. H. R. Skyrme, A Non-linear field theory, *Proc. R. Soc. Lond. A* **260**, no. 1300, 127-138 (1961).

10. T. H. R. Skyrme, A unified field theory of mesons and baryons, *Nucl. Phys.* **31**, 556-569 (1962).

11. A. Chodos, R. L. Jaffe, K. Johnson, C. B. Thorn, V. F. Weisskopf, A new extended model of hadrons. *Phys. Rev D* **9**, 3471-3495 (1974).

12. A. Chodos, R. L. Jaffe, K. Johnson, C. B. Thorn, Baryon structure in the bag theory, *Phys. Rev. D* **10**, no. 8, 2559-2604 (1974).

13. K. Johnson, The M.I.T. bag model, *Acta Phys. Polonica B* **6**, no. 6, 865-892 (1975).

14. T. DeGrand, R. L. Jaffe, K. Johnson, and J. Kiskis, Masses and other parameters of the light hadrons, *Phys. Rev. D* **12**, no. 7, 2060–2076 (1975).

15. M. Rho, A. S. Goldhaber and G. E. Brown, Topological soliton bag model for baryons, *Phys. Rev. Lett.* **51**, 747–750 (1983).

16. M. Bounias and V. Krasnoholovets, Scanning the structure of ill-known spaces: Part 1. Founding principles about mathematical constitution of space, *Kybernetes: The International Journal of Systems & Cybernetics* **32**, no. 7/8, 945-75 (2003); Eds.: L. Feng, B. P. Gibson and Yi Lin; arXiv:physics/0211096.

17. M. Bounias and V. Krasnoholovets, Scanning the structure of ill-known spaces: Part 2. Principles of construction of physical space, *ibid.* **32**, no. 7/8, 976-1004 (2003); Eds.: L. Feng, B. P. Gibson and Yi Lin; arXiv:physics/0212004.

18. M. Bounias and V. Krasnoholovets, Scanning the structure of ill-known spaces: Part 3. Distribution of topological structures at elementary and cosmic scales, *ibid.* **32**, no. 7/8, 1005-20 (2003); Eds.: L. Feng, B. P. Gibson and Yi Lin; arXiv:physics/0301049.

19. M. Bounias and V. Krasnoholovets, The universe from nothing: A mathematical lattice of empty sets. *Int. J. Anticipatory Computing Systems* **16**, 3-24 (2004); Ed.: D. Dubois; arXiv:physics/0309102.

20. V. Krasnoholovets and D. Ivanovsky, Motion of a particle and the vacuum, *Phys. Essays* **6**, no. 4, 554-563 (1993); arXiv.org:quant-ph/9910023.

21. V. Krasnoholovets, Motion of a relativistic particle and the vacuum, *Phys. Essays* **10**, no. 3, 407-416 (1997); arXiv.org:quant-ph/9903077.

22. V. Krasnoholovets, Submicroscopic deterministic quantum mechanics, *Int. J. Comput. Anticipat. Syst.* **11**, 164-179 (2002); Ed.: D. Dubois; arXiv:quant-ph/0109012.

23. V. Krasnoholovets, On the nature of spin, inertia and gravity of a moving canonical particle, *Ind. J. Theor. Phys.* **48**, no. 2, 97-132 (2000); arXiv.org:quant-ph/0103110.

24. V. Krasnoholovets, Variation in mass of entities in condensed media, *Appl. Phys. Research* **2**, no. 1, 46-59 (2010)
http://www.ccsenet.org/journal/index.php/apr/article/view/4287

25. V. Krasnoholovets, On the notion of the photon, *Ann. Fond. L. de Broglie* **27**, no. 1, 93-100 (2002); arXiv:quant-ph/0202170.

26. V. Krasnoholovets, On the nature of the electric charge, *Hadronic J. Suppl.* **18**, no. 4, 425-456 (2003); arXiv:physics/0501132.

27. V. Krasnoholovets, Reasons for nuclear forces in light of the constitution of the real space, *Scientific Inquiry* **7**, no. 1, 25-50 (2006); arXiv:1104.2484 [physics.gen-ph].

28. V. Krasnoholovets, Inerton fields: Very new ideas on fundamental physics, *American Inst. Phys. Conf. Proc.* (Dec. 22, 2010) - Volume **1316**, pp. 244-268. Search for fundamental theory: The VII International Symposium Honoring French Mathematical Physicist Jean-Pierre Vigier (12-14 July 2010, Imperial College, London); Eds.: R. L. Amoroso, P. Rowlands and S. Jeffers; doi:10.1063/1.3536437.

29. F. Wilchek, Asymptotic freedom: From paradox to paradigm, *Proc. Nat. Acad. Sci.* **102**, 8403-8413 (2005); arXiv:hep-th/0502113.

30. D. J. Gross and F. Wilczek, Ultraviolet behavior of non-Abelian gauge theories, *Phys. Rev. Lett.* **30**, 1343–1346 (1973).

31. H. D. Politzer, Reliable perturbative results for strong interactions?, *Phys. Rev. Lett.* **30**, 1346–1349 (1973).

32. H. Fritzsch, The fundamental constants in physics, *Phys. Usp.* **52**, 359-367 (2009); arXiv:0902.2989 [hep-ph].

33. S. Bethke, Experimental tests of asymptotic freedom, *Prog. Part. Nucl .Phys.* **58**, 351-386 (2007); arXiv:hep-ex/0606035.

34. S. Bethke, Data preservation in high energy physics – why, how and when?, *Nucl. Phys. Proc. Suppl.* **207-208**, 156-159 (2010); arXiv:1009.3763 [hep-ex].

35. G. P. Lepage, Lattice QCD for novices, arXiv:hep-lat/0506036.

36. C. Gattringer and C. B. Lang, *Quantum chromodynamics on the lattice: An introductory presentation*, Lect. Notes Phys. 788, Springer, Berlin, Heidelberg (2010), DOI 10.1007/978-3-642-01850-3Y.

37. Y. Makeenko, A brief introduction to Wilson loops and large *N*, arXiv:0906.4487 [hep-th].

38. N. Drukker, Integrable Wilson loops, arXiv:1203.1617 [hep-th].

39. D. Correa, J. Maldacena and A. Sever, The quark anti-quark potential and the cusp anomalous dimension from a TBA equation, arXiv:1203.1913 [hep-th].

40. Y. Aharonov and D. Bohm, Significance of electromagnetic potentials in the quantum theory, *Phys. Rev.* **115**, 485-491 (1959).

41. M. Lüscher and P. Weisz, Quark confinement and the bosonic string, *JHEP* **0207**,049 (2002); arXiv: hep-lat/0207003.

42. K. J. Juge, J. Kuti and C. Morningstar, Fine structure of the QCD string spectrum, *Phys. Rev. Lett.* **90**, 161601 (2003); arXiv:hep-lat/0207004.

43. M. N. Chernodub and F. V. Gubarev, Confining string and its widening in $HP^1$ embedding approach, *Phys. Rev. D* **76**, 016003 (2007); arXiv:hep-lat/0703007.

44. J. Greensite, The confinement problem in lattice gauge theory, *Prog. Part. Nucl. Phys.* **51**, no. 1, 1-83 (2003), arXiv:heplat/0301023.

45. R. Alkofer and J. Greensite, Quark confinement: The hard problem of hadron physics, *J. Phys. G: Nucl. Part. Phys.* **34**, no. 7, S3 (2007); arXiv:hep-th/0610365.

46. G. 't Hooft, Models for confinement, *Progr. Theor. Phys. Suppl.* **167**, 144-154 (2007).

47. G. Hailu, Linear Confinement of quarks from supergravity, arXiv:1107.5827[hep-th].

48. M. S. El Naschie, On quarks confinement and asymptotic freedom, *Chaos, Solitons & Fractals* **37**, no. 5, 1289–1291 (2008).

49. U. Vogl and W. Weise, The Nambu and Jona Lasinio Model: Its implications for hadrons and nuclei, *Progr. Part. Nucl. Phys.* **27**, 195-272 (1991).

50. Review of Particle Properties, *Phys. Rev. D* **45**, S1. Published 1 June 1992.

51. O. Baer, U.-J. Wiese, Can one see the number of colors?, *Nucl. Phys. B* **609**, 225-246 (2001); arXiv:/hep-ph/0105258.

52. R. G. Rajasekaran and S. D. Rindani, Integer-charged quark model and electron-positron annihilation into three jets, *Progr. Theor. Phys.* **67**, no. 5, 1505-1531 (1982).

53. P. M. Ferreira, Can we build a sensible theory with broken charge and colour symmetries?, arXiv: hep-ph/0210024.

54. P. M. Ferreira, Do LEP results suggest that quarks have integer electric charges?, arXiv: hep-ph/0209156.

55. B. A. Kniehl, G. Kramer, B. Pötter, Fragmentation functions for pions, kaons, and protons at next-to-leading order, *Nucl. Phys. B* **582**, 514-536 (2000).

56. B. L. G. Bakker, A. Basset, S. J. Brodsky, W. Broniowski, S. Dalley, T. Frederico, S. D. Glazek, J. R. Hiller, C.-R. Ji, V. Karmanov, D. Kulshreshtha, J.-F. Mathiot, W. Melnitchouk, G. A. Miller, J. Papavassiliou, W. N. Polyzou, N. G. Stefanis, J. P. Vary, A. Ilderton, and T. Heinzl, Light-front quantum chromodynamics. A framework for the analysis of hadron physics, arXiv: 1309.6333 [hep-ph].

57. S. Hartmann, Models and stories in hadron physics, in: *Models as mediators*, M. Morgan and M. Morrison, Eds. (Cambridge University Press, Cambridge, 1999), pp. 326-346.

58. M. Takizawa, K. Tsushima, Y. Kohyama and K. Kubodera, Study of meson properties and quark condensates in the Nambu — Jona-Lasinio model with instanton effects, *Nucl. Phys. A.* **507**, no. 3-4, 611-648 (1990).

59. S. Klevanski, The Nambu–Jona-Lasinio model of quantum chromodynamics, *Rev. Mod. Phys.* **64**, no. 3, 649–708 (1992).

60. I. C. Cloet, W. Bentz and A. W. Thomas, Role of diquark correlations and the pion cloud in nucleon elastic form factors, *Phys. Rev. C* **90**, 045202 (2014); arXiv:1405.5542 [nucl-th].

61. S. Yasui and A. Hosaka, Quark droplets with chiral symmetry in the Nambu–Jona-Lasinio model, arXiv: hep-ph/0604206.

62. S. M. H. Wong, What exactly is a Skyrmion?, arXiv:hep-ph/0202250.

63. H. Weigel, Baryons as three flavor solitons *Int. J. Mod. Phys. A* **11**, 2419-2544 (1996).

64. R. Ouyed and M. Butler, Skyrmion stars, *Astrophys. J.* **522**, 453-459 (1999).

65. P. Jaikumar, M. Bagchi and R. Ouyed, High-density skyrmion matter and neutron stars, *Astrophys. J.* **678**, 360-368 (2008).

66. J. Jäykkä, M. Speight and P. Sutcliffe, Broken baby Skyrmions, *Proc. R. Soc. A* **468**, no. 2140, 1085-1104 (2012).

67. P. Hasenfratz and J. Kuti, The quark bag model, *Phys. Reports* **40**, no. 2, 75-179 (1978).

68. C. DeTar and J. Donoghue, Bag models of hadrons, *Annual Review of Nuclear and Particle Science*, **33**, 235–264 (1983).

69. Y. Iwamura and Y. Nogami, Deformed baryons: Constituent quark model *vs.* bag model, *Il Nuovo Cimento A* **89**, no. 3, 315-323 (1985).

70. R. Bhaduri, *Models of the nucleon. From quarks to soliton* (Redwood City: Addison-Wesley Publishing Company, 1988).

71. A. Abbas, The MIT bag model and the spin structure of the nucleon, *J. Phys. G: Nucl. Part. Phys.* **15,** No. 7, L129-L133 (1989).

72. A. Hosaka and H. Toki, *Quarks, baryons and chiral symmetry* (World Scientific, 2001).

73. J. Jäykkä, *On topological solitons in the Faddeev-Skyrme model and its extensions*, SARJA - Ser. A1, OSA - Tom. **399**; Astronomica-Chemica-Physica-Mathematica, Annales Universitatis Turkuensis (Turun, Yliopisto, Turku, 2009).

74. D. Gomez Dumm, A. J. Garcia and N. N. Scoccola, Non-leptonic decays of hyperons in the Skyrme model, in *International workshop on hadron physics 2000: Topics on the structure and interaction of hadron systems* (World Scientific, 2001), pp. 310-313.

75. K. Tsushima, D. O. Riska, Dilatons in the topological soliton model for the hyperons, *Nucl. Phys. A* **560**, no. 4, 985-996 (1993).

76. A. Vilenkin, Cosmic strings and domain walls, *Phys. Rep.* **121**, no. 5, 263-315 (1985).

77. L. B. Okun, The concept of mass. Mass, energy, relativity, *Uspekhi Fiz. Nauk* **158**, no. 3, 511 (1989); in Muscovian.

78. F. Wilczek, The origin of mass, *Mod. Phys. Lett.* A **21**, no. 9, 701-12 (2006).

79. L. de Broglie, *Les incertitudes d'Heisenberg et l'interprétation probabiliste de la méchanique Ondulatoire* (Gauthier-Villars, Bordas, Paris, 1982); Chapter 2, sect. 4.

80. D. ter Haar, *Elements of Hamiltonian mechanics*, 2nd edition (Pergamon Press, 1971), section 8.2.

81. M. Born, Das Adiabatenprinzip in der Quantenmechanik, *Zeitschrift für Physik* **40**, 167-192 (1926).

82. M. Born, The statistical interpretation of quantum mechanics. Nobel Lecture, December 11, 1954, in *Nobel Lectures, Physics 1942-1962*, Elsevier Publishing Company, Amsterdam (1964), pp. 256-267.

83. H. Poincaré, Sur la dynamique de l'électron, *Rendiconti del Circolo matematico di Palermo* **21**, 129-176 (1906); also: *Oeuvres*, t. **IX**, 494-550].

84. Ya. E. Geguzin, *Bubbles* (Nauka, Moscow, 1985), p. 41; in Muscovian.

85. R. Miskimen, Neutral pion decay, *Ann. Rev. Nucl. Particle Sci.* **61**, 1-21 (2011).

86. N. Van Hieu, *Lectures on the theory of unitary symmetry in elementary particle physics* (Atomizdat, Moscow, 1967), 344 p.; in Muscovian.

87. Yu. B. Rumer and A. I. Fet, *The theory of unitary symmetry* (Nauka, Moscow, 1970); in Muscovian.

88. Y. Nambu, *Quarks: frontiers in elementary particle physics* (World Scientific, Singapore, 1985).

89. C. Csaki, Yu. Shirman and J. Terning, A Seiberg dual for the MSSM: partially composite W and Z, *Phys. Rev. D* **84**, 095011 (2011); arXiv:1106.3074 [hep-ph].

90. A. G. Cohen and S. L. Glashow, New constraints on neutrino velocities, arXiv:1109.6562 [hep-th].

91. R. Friedberg and T. D. Lee, Fermion-field nontopological solitons. II. Models for hadrons, *Phys. Rev. D* **16**, 1096–1118 (1977).

92. C. Wu, W.-L. Qian and R.-K. Su, Improved density-dependent quark mass model with quark-$\sigma$ meson and quark-$\omega$ omega meson couplings, *Phys. Rev. C* **77**, 015203 (2008).

93. S. Nagai, T. Miyatsu, K. Saito and K. Tsushima, Quark-meson coupling model with the cloudy bag, *Phys. Lett. B* **666**, 239-244 (2008); arXiv:0803.4362 [nucl-th].

94. G. Holzwarth, Electromagnetic form factors of the nucleon in chiral soliton models, in *The multifaceted Skyrmion*; Eds.: G. E. Brown and M. Rho (World Scientific, Singapore, 2010), pp. 41-55.

95. P. A. M. Guichon, H. H. Matevosyan, N. Sandulescu and A. W. Thomas, Physical origin of density dependent force of the Skyrme type within the quark meson coupling model, *Nucl. Phys. A* **772**, nos. 1-2, 1-19 (2006); arXiv:nucl-th/0603044.

96. M. Wakamatsu, Can the $SU(3)$ chiral quark soliton model describe the nucleon properties better than the $SU(2)$ model?, *Phys. Rev. D* **54**, 2161-2167 (1996).

97. F. Huang, Z.-Y. Zhang and W.-Y. Yu, KN phase shifts in chiral $SU(3)$ quark model, *Commun. Theor. Phys.* **42**, no. 4, 557-580 (2004).

98. Ch. Wu and R.-K. Su, Quark deconfinement phase transition for the improved quark mass density-dependent model, *J. Phys. G: Nucl. Part. Phys.* **35**, no. 12, 125001 (2008).

99. V. Mantovani-Sarti, A. Drago, V. Vento and B.-Y. Park, The baryon number two system in the Chiral Soliton Model, arXiv:1201.0675 [nucl-th].

100. E. Comay, The Yukawa Lagrangian density is inconsistent with the Hamiltonian, *Apeiron* **14**, no. 1, 1-11 (2007), http://redshift.vif.com/JournalFiles/V14NO1PDF/V14N1COM.pdf

101. R. Gilman and F. Gross, Electromagnetic structure of the deuteron, *J. Phys. G: Nucl. Part. Phys.* **28**, R37-R116 (2002).

102. R. M. Santilli, *Foundations of hadronic chemistry with applications to new clean energies and fuels* (Kluwer Academic Publisher, Boston-Dordrecht-London, 2001).

103. A. A. Sokolov, Yu. M. Loskutov and I. M. Ternov, *Quantum mechanics* (Prosveshchenie, Moscow, 1965), p. 222; in Muscovian.

104. M. Islam, R. Luddy, J. Kaspar and A. Prokudin, Picturing the proton by elastic scattering, *CERN Courier* **49**, no. 10, 35 (2009) December.

105. M. M. Islam, J. Kašpar, R. J. Luddy and A. V. Prokudin, Proton-proton elastic scattering at LHC and proton structure, in *13th International Conference on Elastic and Diffractive Scattering: Moving Forward into the LHC Era*, CERN, Geneva, Switzerland, 29 Jun - 03 Jul (2009), pp. 48-54 *CERN Document Server*, http://cdsweb.cern.ch/record/1247028

106. M. M. Islam, J. Kašpar and R. J. Luddy, Proton Structure and Prediction of Elastic Scattering at LHC at Center-of-Mass Energy 7 TeV, *Proc. Eleventh Workshop Non-Perturbat. Quant. Chromodynamics*, l'Institut Astrophysique de Paris June 6-10, 2011; Eds.: B. Mueller, M. A. Rotondo and Ch.-I Tan; http://www.slac.stanford.edu/econf/C1106064/.

107. F. L. Braghin, Skyrmion and chiral symmetry breaking, *AIP Conf. Proc.* **739**, 678-680 (2004).

108. I. T. Lorenz, H.-W. Hammer and U.-G. Mei$\beta$ner, The size of the proton: Closing in on the radius puzzle, *Eur. Phys. J. A: Hadr. and Nucl.* **48**, no. 11, 1-5 (151) (2012).

109. R. Pohl, R. Gilman, G. A. Miller and K. Pachucki, Muonic hydrogen and the proton radius puzzle, arXiv:1301.0905 [physics.atom-ph] (2013).

110. J. C. Bernauer and R. Pohl, The proton radius puzzle. Two experiments have come up with two widely different values for the proton's radius. What's going on? *Scientific American* **310**, no. 2, February 2014, pp. 18-25.

111. S. T. Thornton and A. Rex, *Modern physics for scientists and engineers*, 4th Edition (Brooks/Cole, 2011), p. 436.

112. O. H. Sytenko and V. K. Tartakovsky, *The theory of nucleus* (Lybid, Kyiv, 2000), p. 8; in Ukrainian.

113. S. E. Kuhn, J.-P. Chen and E. Leader, Spin structure of the nucleon - status and recent results, *Prog. Part. Nucl. Phys.* **63**, 1-50 (2009); arXiv:0812.3535 [hep-ph].

114. A. Adare et al. (PHENIX Collaboration). Cross section and parity-violating spin asymmetries of W$^\pm$ boson production in polarized $p + p$ collisions at $\sqrt{s} = 500$ GeV, *Phys. Rev. Lett.* **106**, no. 6, 062001 (2011) [6 pages].

115. M. M. Aggarwal et al. (STAR Collaboration). Measurement of the parity-violating longitudinal single-spin asymmetry for W$^\pm$ boson production in polarized proton-proton collisions at $\sqrt{s} = 500$ GeV, *Phys. Rev. Lett.* **106**, no. 6, 062002 (2011) [6 pages].

116. E. Comay, Spin, isospin and strong interaction dynamic, arXiv:1107.4688 [physics.gen-ph].

117. E. Comay, Theoretical errors in contemporary physics, arXiv:physics/0509071 [physics.gen-ph].

118. E. Comay, A regular monopole theory and its application to strong interactions, in *Has the last word been said on classical electrodynamics?* (Rinton Press, NJ, 2004); arXiv:physics/0405050.

119. V. Krasnoholovets, Submicroscopic viewpoint on gravitation, cosmology, dark energy and dark matter, and the first data of inerton astronomy, in *Recent Developments in Dark Matter Research*; Eds.: N. Kinjo and A. Nakajima (Nova Science Publishers, 2014), pp. 1-61 (ISBN: 978-1-62948-010-7).

120. E. Storms, *The science of low energy nuclear reaction. A comprehensive compilation of evidence and explanations about cold fusion* (World Scientific, 2007).

121. C. L. Kervran, *Biological transmutations*, second printing, J. de Langre, Ed. (Happiness Press, Magalia, California, 1998).